Atypical collective oscillatory activity in cardiac tissue uncovered by optogenetics

Alexander S. Teplenin[1*], Nina N. Kudryashova[1§], Rupamanjari Majumder[1¶], Antoine A.F. de Vries[1], Alexander V. Panfilov[1,2], Daniël Pijnappels[1†*], Tim De Coster[1,3†*]

***For correspondence:**
a.teplenin@lumc.nl (AST);
d.a.pijnappels@lumc.nl (DAP);
t.j.c.de_coster@lumc.nl (TDC)

[†]These authors contributed equally to this work

Present address: [§]Institute for Adaptive and Neural Computation, Informatics Forum, School of Informatics, the University of Edinburgh, Edinburgh, United Kingdom; [¶]Nantes Université, INSERM, l'institut Du Thorax, Nantes, France

[1]Laboratory of Experimental Cardiology, Department of Cardiology, Heart Lung Center Leiden, Leiden University Medical Center, 2333 ZA Leiden, the Netherlands;
[2]Department of Physics and Astronomy, Ghent University, 9000 Ghent, Belgium;
[3]Netherlands Heart Institute, 3511 EP Utrecht, the Netherlands

Abstract Many biological processes emerge as frequency-dependent responses to trains of external stimuli. Heart rhythm disturbances, i.e. cardiac arrhythmias, are important examples as they are often triggered by specific patterns of preceding stimuli. In this study, we investigated how ectopic arrhythmias can be induced by external stimuli in cardiac tissue containing a localised area of depolarisation. Using optogenetic *in vitro* experiments and *in silico* modelling, we systematically explored the dynamics of these arrhythmias, which are characterized by local oscillatory activity, by gradually altering the degree of depolarization in a predefined region. Our findings reveal a bi-stable system, in which transitions between oscillatory ectopic activity and a quiescent state can be precisely controlled, i.e. by adjusting the number and frequency of propagating waves through the depolarized area oscillations could be turned on or off. These frequency-dependent responses arise from collective mechanisms involving stable, non-self-oscillatory cells, contrasting with the typical role of self-oscillations in individual units within biophysical systems. To further generalize these findings, we demonstrated similar frequency selectivity and bi-stability in a simplified reaction-diffusion model. This suggests that complex ionic cell dynamics are not required to reproduce these effects; rather, simpler non-linear systems can replicate similar behaviour, potentially extending beyond the cardiac context.

Introduction

Biological systems like the heart typically display complex dynamical behaviour through interactions among components such as genes, proteins, or cells (***Dana et al.*** (***2008***)). These systems exhibit non-linear dynamics, feedback loops, and adaptability, reflecting phenomena like homeostasis, evolution, and rhythm stability (***Xiong and Garfinkel*** (***2023***)). Central to the framework of dynamical systems is the concept of the phase space, a multidimensional representation in which each point corresponds to a unique state of the system. In geography when a small ball rolls on a raised-relief map, a state would include the planar position, elevation, speed and acceleration of the ball.

Within the phase space, the long-term behaviour of a system can often be described in terms of attractors, which are subsets of the phase space that trajectories tend toward over time. At-

tractors can take various forms, including fixed points, periodic orbits, and chaotic sets, reflecting the rich diversity of behaviours possible in dynamical systems. By replacing the ball by local rain in the raised-relief map, rivers, lakes and other bodies of water are attractors where that rain is collected. A watershed, also known as a drainage basin, is an area of land where any rain that falls will drain into the same river, lake or body of water. Therefore they are basins of attraction. Mountain ridges are separatrices that divide the watersheds, or more formally theoretical surfaces that divide the phase space into different basins of attraction. A separatrix therefore denotes the transition between different regions of the phase space. The terminology introduced here comes back throughout our paper, with the addition of a "state", i.e. one of the attractors in the system. When the system is not interacted with, it will stay at the same point(s) in phase space.

Some systems only have a single basin of attraction. However, in others the phenomenon of bi-stability emerges, where two distinct attractors coexist, each with its own basin of attraction. Bi-stability is a hallmark of many natural and engineered systems, from climate dynamics to neural networks, ecological models, and cardiac dynamics (***Angeli et al.*** (***2004***)). The interplay between basins in such systems can give rise to complex behaviours, making the characterization of these basins a critical component of a system's analysis.

In this manuscript, the focus is on the complex system of the heart. At rest, ventricular cardiomyocytes (i.e muscle cells of the lower heart chamber) have a membrane potential of -80 to -90 mV. This resting state is an attractor of the system. When pushed out of equilibrium (e.g. due to an influx of Na^+ ions or electrical stimulation), cardiomyocytes first depolarize and subsequently get attracted again towards the resting state by an efflux of K^+ ions. In phase space the trajectory that gets mapped out resembles a cycle, corresponding to one heartbeat. When multiple of these cells are connected to each other, emergent behaviour can arise. Within this dynamic system of cardiomyocytes, we investigated emergent bi-stability in cell monolayers under the influence of spatial depolarization patterns. By using a train of external (electrical) waves, the system could be actively moved from one basin of attraction to another.

Cardiac arrhythmias are typically initiated by specific triggers, with point-source waves, i.e. ectopic waves being the most prevalent. To study ectopy in laboratory settings, control needs to be exerted over the depolarisation of cardiomyocytes. This can be achieved by optogenetics, i.e. a biological technique to control the activity of cells with light. This approach relies on the introduction of recombinant genes encoding light-activatable proteins into cells to endow them with a new biological function (***Tan et al.*** (***2022***)). One way to depolarise a cardiomyocyte is by using mini-singlet oxygen generator (miniSOG). Upon activation with blue light, miniSOG converts molecular oxygen from its ground state ($^3O_2$) into highly reactive singlet oxygen ($^1O_2$). The resulting oxidative damage induces a state of prolonged depolarisation in cardiomyocytes following electrical stimulation (***Jangsangthong et al.*** (***2016***)). In such a system, it was previously observed that spatiotemporal illumination can give rise to collective behaviour and ectopic waves (***Teplenin et al.*** (***2018***)) originating from illuminated/depolarised regions (with high curvature). These waves resulted from the interplay between the diffusion current and the bi-stable state that was induced in the illuminated region.

Although miniSOG can create depolarised areas, it is difficult to control the process precisely since it depolarises cardiomyocytes through an indirect pathway. Therefore, in this manuscript, we used light-sensitive ion channels to obtain more refined control over cardiomyocyte depolarisation. These ion channels allow the cells to respond to specific wavelengths of light, facilitating either depolarization or hyperpolarisation (***Ördög et al.*** (***2021***, 2023)) through a direct pathway. By inducing cardiomyocyte depolarisation or hyperpolarisation only in the illuminated areas, optogenetics enables precise spatiotemporal control of cardiac excitability, an attribute we exploit in this manuscript (***Appendix 2 Figure 1***). With the aid of the light-gated ion channel CheRiff (***Hochbaum et al.*** (***2014***)), ectopic waves similar to those obtained in the miniSOG system could be elicited (***Appendix 2 Figure 2***). Due to the superior control over depolarisation imposed by CheRiff, we uncovered new effects and unobserved behaviour related to the transition from a mono-stable cardiac

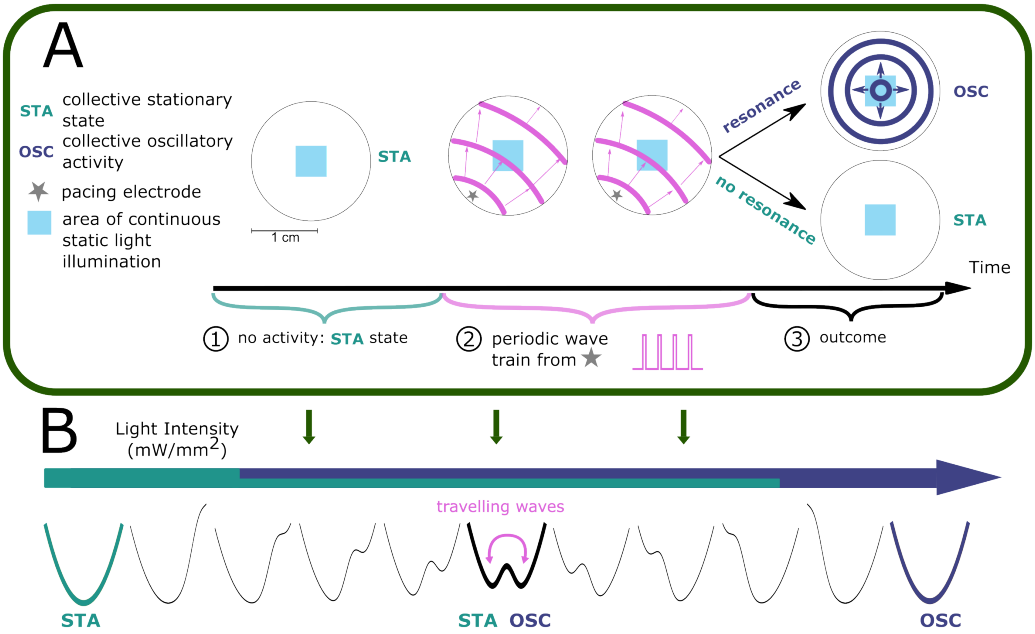

Figure 1. Bi-stability between stationary behaviour and collective oscillations. **(A)** Experimental timeline for a monolayer of optogenetically modified NRVMs under constant illumination of its center: 1) observation of a collective stationary state (STA); 2) periodic wave train from the pacing electrode; 3) outcome observation of collective behaviour, either stationary (STA) or oscillatory (OSC). **(B)** Light intensity influences collective behaviour of excitable systems, transitioning between a stationary state (STA) at low illumination intensities and an oscillatory state (OSC) at high illumination intensities. Bi-stability occurs at intermediate light intensities, where transitions between states are dependent on periodic wave train properties. TR. OSC, transient oscillations.

system to a bi-stable one that displays periodic oscillations. This transition resulted from the interaction of an illuminated region with depolarized cardiomyocytes and an external wave train. More specifically, we found that our system displayed frequency selectivity: it oscillated only as a reaction to a specific range of inter-pulse external stimuli times. In neuroscience, this behaviour is classified as "resonance". However, to avoid confusion with classical resonance, where the strength of the response is dependent on the input, here the phenomenon is called "induced pacemaker activity". Evidence for this induced pacemaker activity will be presented both *in vitro* and *in silico*.

Results

Bi-stability in cardiomyocyte monolayers was realised both *in vitro* and *in silico* (***Figure 1***). *In vitro* this happened through patterned illumination applied to neonatal rat ventricular myocyte (NRVM) monolayers, which were optogenetically modified using the blue light-activatable cation channel CheRiff (***Appendix 2 Figure 1***). *In silico*, use was made of a slightly modified (see Methods and Materials) NRVM computational model (***Majumder et al.*** (***2016***)) complemented with a model for a depolarising light-gated ion channel (***Williams et al.*** (***2013***)). In both cases, the illumination pattern consisted of a rectangle of variable light intensities. After initiating a periodic wave train (of variable pulse number and interpulse interval/period) from a pacing electrode, two main outcomes and one special case were observed (***Figure 1***A). The first outcome was that the tissue stayed in the stationary rest state (STA). The second outcome was that the illuminated region became a pacemaker, which sent out pulses from its edges as a form of oscillatory behaviour (OSC). The special case consisted of an in-between case, in which the illuminated region only sends out a limited amount of pulses before returning to the stationary state thus showing transient oscillatory behaviour (TR. OSC). Except for the occasional mention, this last behaviour of transient oscillations will be re-

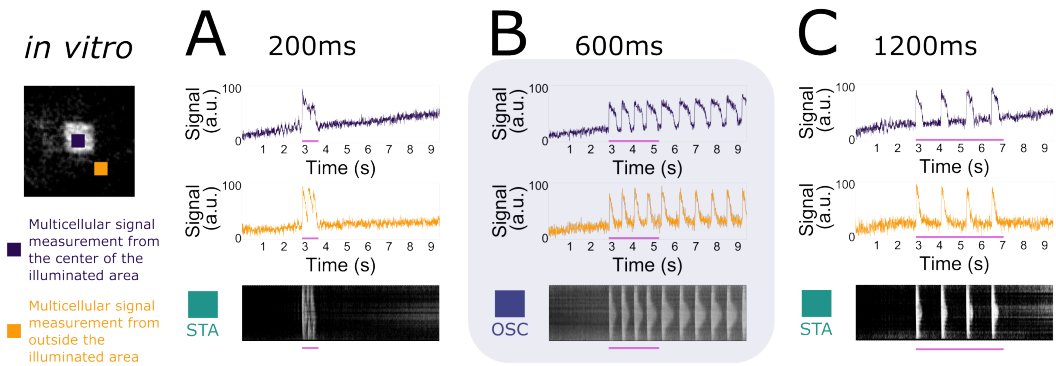

Figure 2. Frequency dependency of induced collective pacemaker activity. *In vitro* monolayers of optogenetically modified NRVMs show that the transition from the stationary state (STA) towards the oscillatory state (OSC) is dependent on the frequency of excitatory waves passing through an illuminated area under a constant number of 4 pulses. **(A)** Four pulses at high frequency (200 ms) are not enough to induce the transition. **(B)** Four pulses at medium frequency (600 ms) are sufficient to induce the transition. **(C)** Four pulses at low frequency (1200 ms) fail once again in inducing the transition.

served for more detailed discussion in the supplement. All light intensity-influenced monolayer behaviours are visualised together in ***Appendix 2 Figure 3***. Here, we will focus on the two main behaviours after periodic wave trains: STA and OSC. As shown below, these two behaviours can exist within the same monolayer under bi-stability and transitions from one state to the other are possible using periodic wave trains. The occurrence of this phenomenon appears to be influenced by the light intensity applied to the illuminated region (***Figure 1***B). In a step-by-step manner, we unravelled the intricacies of this tissue level (i.e. collective) bi-stability between oscillatory and stationary behaviour, linking experiment to theory.

In vitro realisation of collective light-induced bi-stability

To test the scope of collective bi-stability *in vitro*, multiple parameters were varied within our experimental set-up. The first one of these was the frequency of stimulation, visualised in ***Figure 2***, where the number of electrical pulses and the light intensity (in the range 0.03125-0.25 mW/mm^2) were kept fixed. In every NRVM monolayer (26 biological replicates/monolayers), three frequencies (stimulation periods 200, 600, and 1200 ms) were tested subsequently, with a total of three repetitions (technical replicates) of the full set, totalling $26 \times 3 = 78$ observations at each pacing frequency. Optical voltage signals were measured both at the center of the illuminated area (top traces) as well as in the bulk of the tissue (bottom traces), in order to visualise action potentials throughout the tissue. Underneath these optical voltage traces is a space-time plot of the experimental monolayer, the vertical axis showing space and the horizontal one showing time. At each moment in time, the middle line of the monolayer image was plotted. White shows depolarized tissue, while black signifies repolarised cells. From these plots, intermediate stimulation periods (600 ms) were observed to change the monolayer from a collective stationary state to a collective oscillatory state, while low (200 ms) or high (1200 ms) ones had no effect. It was observed that the oscillatory state consisted of ectopic pacemaker activity with a frequency (735 ms-period) that was different from the stimulus train frequency (600-ms period). Similar results were found for the transient oscillatory state (***Appendix 2 Figure 4***A). In short, we found that collective bi-stability becomes apparent in the mid-range of electrical pacing frequencies.

A second parameter tested was the number of pulses, visualised in ***Figure 3***, where the period of stimulation (600 ms) and the light intensity (in the range 0.03125-0.25 mW/mm^2) were kept fixed. In every NRVM monolayer (7 biological replicates/monolayers), two different pulse numbers (2 and 4) were tested subsequently, with a total of three repetitions (technical replicates) of the full set,

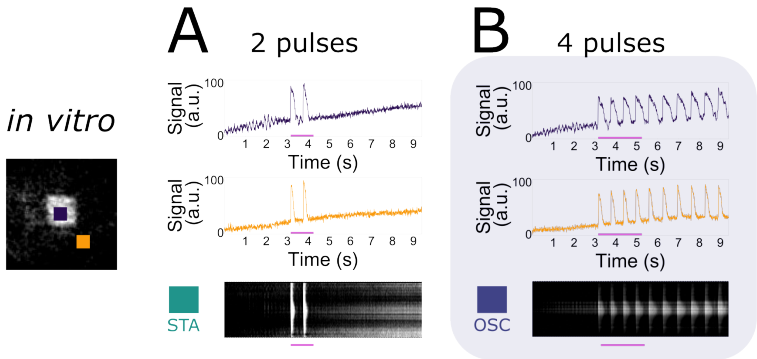

Figure 3. Accumulation of pulses to induce collective pacemaker activity. *In vitro* monolayers of optogenetically modified NRVMs show that the transition from the stationary state (STA) towards the oscillatory state (OSC) is dependent on the number of excitatory waves passing through an illuminated area at a constant electrical pacing frequency of 600 ms. **(A)** Two pulses are not enough to induce the transition. **(B)** Four pulses are sufficient to induce the transition.

totalling $7 \times 3 = 21$ observations for each number of pulses. Once again optical voltage traces were taken from the center of the illuminated area and from the bulk of the tissue. Our observations show that a minimum number of pulses is needed to change the collective behaviour of the monolayer from stationary to oscillatory.

Taken together, we found a way to control transitions of collective behaviour of cardiomyocyte monolayers from stationary to oscillatory through two different parameters, i.e. the frequency and number of pulses.

In silico realisation of collective light-induced bi-stability

Using the power of state-of-the-art computational modelling, we performed similar experiments to the *in vitro* ones with a modified version of the ***Majumder et al.*** (***2016***) model for NRVMs combined with the ***Williams et al.*** (***2013***) model for the H134R mutant of *Chlamydomonas reinhardtii* channelrhodopsin-2. As this light-sensitive ion channel slightly differs from CheRiff in its biophysical properties, the *in vitro* findings will have a qualitative rather than a quantitative correspondence to the *in silico* results, which are visualised in ***Figure 4***. Under fixed constant illumination (1.7124 mW/mm^2) and a fixed number of 4 pulses, frequency dependency of collective bi-stability was reproduced in ***Figure 4***A. Once again, only intermediate electrical pacing frequencies (500-ms period) caused transitions from collective stationary behaviour to collective oscillatory behaviour and ectopic pacemaker activity had periods (710 ms) that were different from the stimulation train period (500 ms). ***Figure 4***B shows the accumulation of pulses necessary to invoke a transition from the collective stationary state to the collective oscillatory state at a fixed stimulation period (600 ms). Once more, ectopic pacemaker activity had periods (750 ms) that were different from the stimulation train period (600 ms). Also for the transient oscillatory state, the simulations show frequency selectivity (***Appendix 2 Figure 4***B).

Having established a qualitative correspondence between the *in silico* model and *in vitro* experiments, the unique properties of the computational model were exploited to assert control over all variables in order to determine the parameter ranges of the state transitions. We previously identified three important parameters influencing such transitions: illumination strength, number of pulses, and frequency of pulses. Scanning through all three variables revealed the specific conditions at which transition from the stationary state towards the oscillatory state occurred as shown in the rightmost panel of ***Figure 4***C with slices for fixed illumination extracted from this 3D-plot shown at the left. With increasing light intensity, the parameter range (pulse and period) in which bi-stability can be detected increases (the total area of TR.OSC. + OSC. becomes larger), and

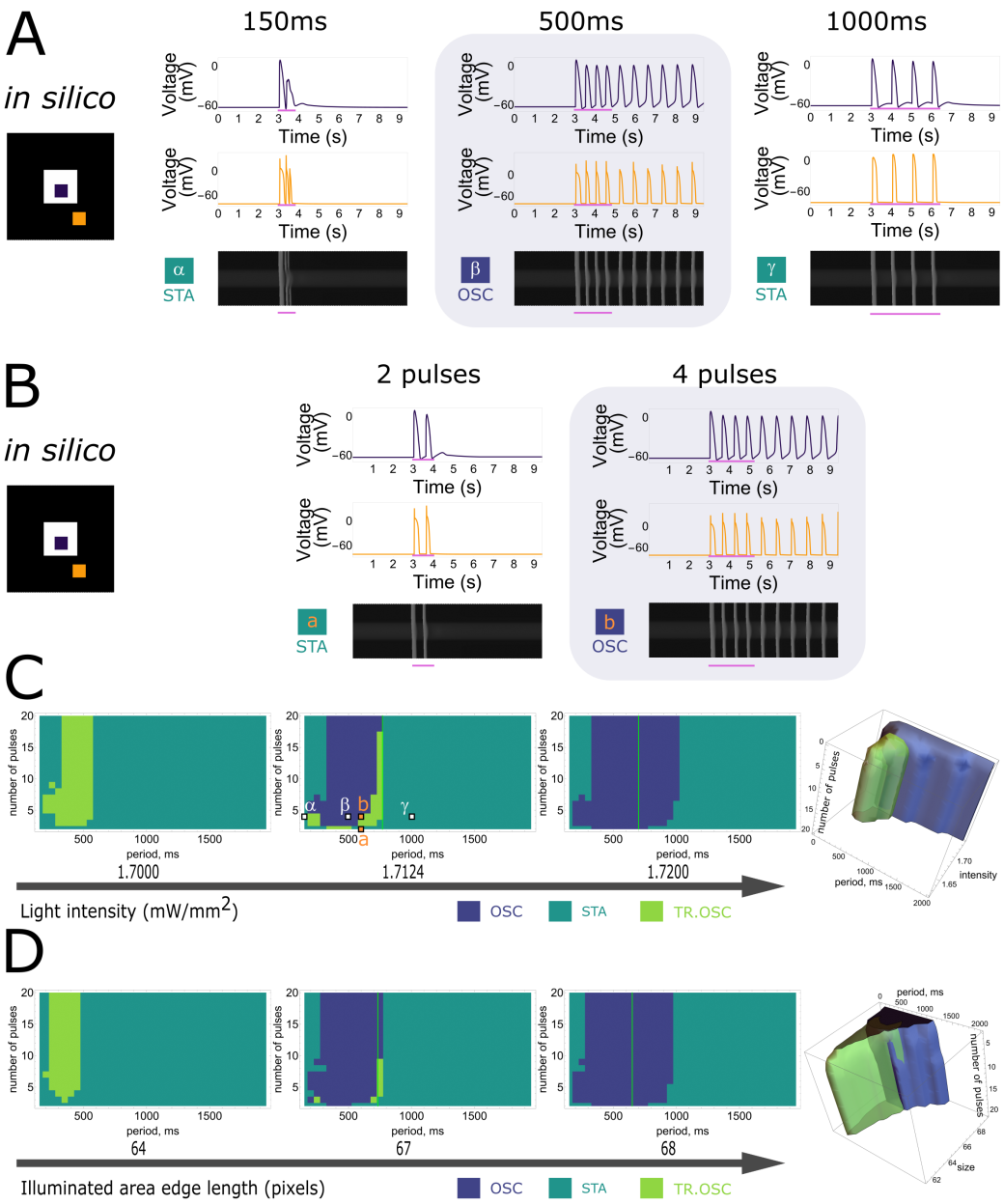

Figure 4. *In silico* demonstration of frequency dependency and accumulation of pulses to induce collective pacemaker activity similar to that observed *in vitro*. (A) Monolayers of optogenetically modified NRVMs show that the transition from the stationary state (STA) towards the oscillatory state (OSC) is dependent on the frequency of excitatory waves passing through an illuminated area under a constant number of 4 pulses. From left to right: no induction at stimulation periods of 150 and 1000 ms, induction at a stimulation period of 500 ms. **(B)** Monolayers of optogenetically modified NRVMs show that the transition from the stationary state towards the oscillatory state is dependent on the number of excitatory waves passing through an illuminated area under a constant frequency (600-ms period). From left to right: no induction at 2 pulses, induction at 4 pulses. **(C)** Three-dimensional parameter scan of all variables (light intensity, pacing period, and number of pulses) showing how dependency on period and on number of pulses relate to each other. Representative slices for fixed light intensities are displayed at the left. Vertical green lines show the natural pacemaker frequency the monolayer settles to after initiation of pacemaker activity. Letters in the middle panel correspond to traces in **A** and **B**. **(D)** Three-dimensional parameter diagram in which the size of the illuminated area was varied instead of the light intensity. Representative slices for fixed area edge lengths are displayed at the left. Vertical green lines show the natural pacemaker frequency the monolayer settles to after initiation of pacemaker activity.

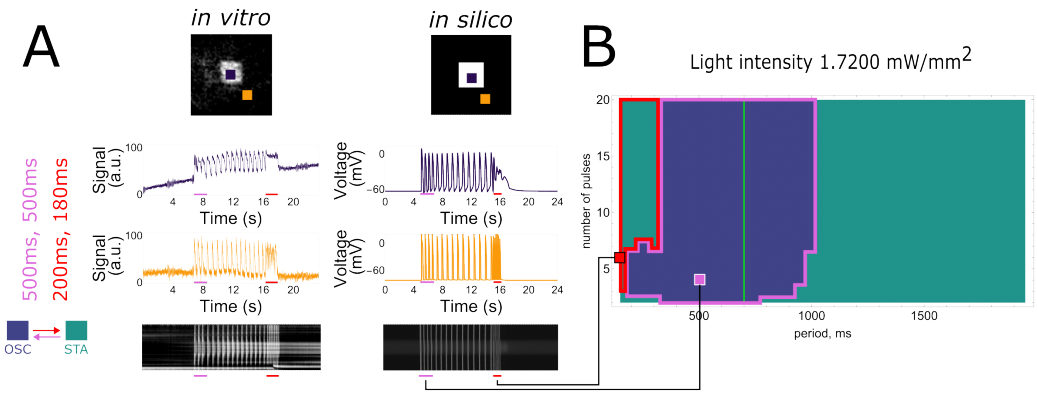

Figure 5. Demonstration of frequency dependency to terminate collective pacemaker activity. (A) Initiation and termination of collective pacemaker activity *in vitro* (left panel, 3 pulses of 500-ms period for initiation, 8 pulses of 200-ms period for termination) and *in silico* (right panel, 4 pulses of 500-ms period for initiation, 7 pulses of 180-ms period for termination). **(B)** Rightmost slice from ***Figure 4***C showing *in silico* experiments at a fixed light intensity (1.72 mW/mm^2) and size of the illuminated area (67 pixels edge length) with indicated termination (red border) and initiation (magenta border) period ranges. Vertical green line shows the natural pacemaker frequency the monolayer settles to after initiation of pacemaker activity.

transient oscillatory states transition towards oscillatory states.

Except for the three aforementioned parameters, a fourth one was found to have an influence on the state transitions: the size of the illuminated region. Also this parameter was first tested *in vitro* resulting in 5 biological replicates/monolayers showing transitions to the oscillatory state and 6 biological replicates/monolayers showing transient oscillations. The effect of the size of the illuminated area on the occurrence of bi-stability was qualitatively reproduced *in silico* (***Appendix 2 Figure 5***). Varying the number and frequency of pulses together with the illuminated area at a fixed light intensity of 1.7200 mW/mm^2 resulted in the dynamic behaviour shown in ***Figure 4***D. For the conditions that resulted in stable oscillations, the green vertical lines in the middle and right slices represent the natural pacemaker frequency in the oscillatory state. After the transition from the stationary towards the oscillatory state, the illuminated region settles into this period of sending out pulses. The location of this line depends on the light intensity and the size of the illuminated region. However, it is independent of the number of pulses and the frequency of the stimulus train. Figures ***Figure 4***C and ***Figure 4***D also illustrate that no oscillatory state could be induced with a high number of pulses for stimulus trains of high frequency (i.e. low stimulation period).

Termination of collective pacemaker activity

A closer look at the high frequency range showed that it not only prevented the initiation of ectopic pacemaker activity, but can also cause its termination (***Figure 5***A). In NRVM monolayers (3 biological replicates/monolayers), collective ectopic pacemaker activity was first initiated using a stimulus train of 3 pulses with a period of 500 ms. Once ongoing, 8 pulses in the high frequency range (period 200 ms) terminated the ectopic pacemaker activity and made the tissue go back to its resting state. When copying this experimental protocol *in silico*, qualitative correspondence was shown using 4 pulses with a period of 500 ms to initiate pacemaker activity, and 7 pulses with a period of 180 ms to terminate it. Note that both experimentally and computationally every pulse of the stimulus train is captured (orange traces), despite the fact that the voltage traces from points inside the illuminated region do not give that impression.

Once again, the qualitative *in silico* correspondence allows us to determine the specific conditions at which initiation and termination of collective ectopic pacemaker activity occur in more detail (***Figure 5***B). In the period vs. number of pulses plot, which is a copy of the rightmost slice

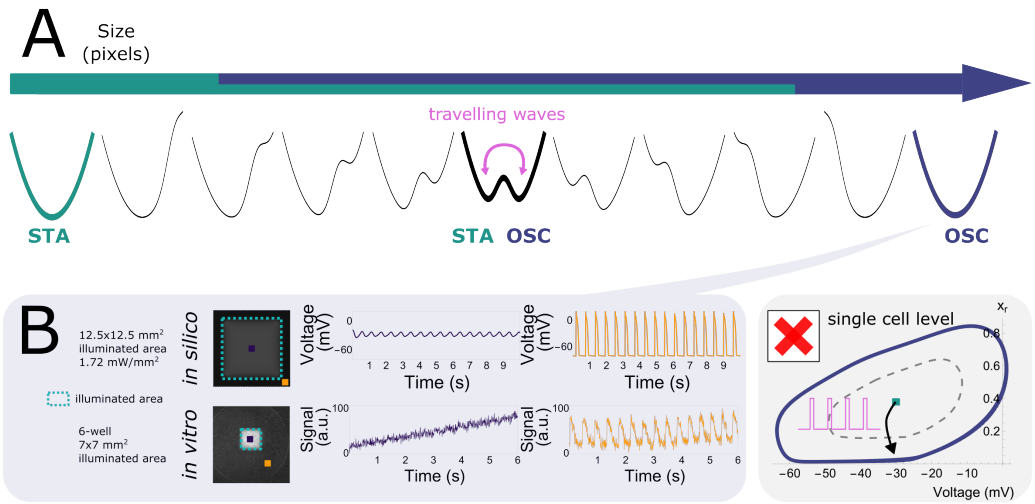

Figure 6. Wave train-induced pacemaker activity is a multicellular collective phenomenon. (A) Illuminated area (under constant light intensity) influences collective behaviour of excitable systems, transitioning between a stationary state for small illuminated areas and an oscillatory state for large illuminated areas. **(B)** In the oscillatory regime (large illuminated areas), illuminated cells in the center (purple traces) are depolarised (both *in silico* and *in vitro*), while oscillatory behaviour still takes place in the bulk of the tissue (orange traces). This discards the simplest model of bi-stable limit cycles at the single cell level.

in ***Figure 4***C, the region showing termination (red-lined) did not overlap with the region showing initiation (magenta-lined).

The collective nature of wave train-induced pacemaker activity

After exploring collective bi-stability in practice, we aimed to gain a deeper understanding of this phenomenon. Bi-stability is a wide-spread phenomenon and can take place at the single cell level (***Guevara*** (***2003***)), which would be the simplest assumption for our monolayer system as well. When this would be the case, all cells would become oscillatory under illumination. We tested this hypothesis by making use of one of the four parameters we investigated earlier: the illuminated area. This parameter shows a transition from the stationary state towards the oscillatory state (***Figure 6***A) just like the light intensity parameter (***Figure 1***B) resulting in spontaneous oscillatory behaviour with waves emanating from the center of the illuminated area for a large area size and at a constant low light intensity (***Figure 4***D). These circumstances allowed us to compare the voltage traces between the center of the irradiated area and the bulk of the tissue, both *in vitro* and *in silico*. While the cells outside of the illuminated area showed oscillating membrane potentials those in the center of the illuminated region, i.e. those least affected by the coupling current of neighbouring cells, displayed a stable elevation of membrane potential. Hence, this implies that not all illuminated cells became oscillatory. We can therefore reject the simplest hypothesis of bi-stability at the single cell level, but have to speak of a collective phenomenon. It is for this reason that throughout the manuscript the observed effects are referred to as "collective" pacemaker activity.

Insight into pulse-dependent collective state transitions

Knowing that we are dealing with a collective phenomenon, we wanted to gain a deeper understanding in the observed pulse-dependent collective transitions from stationary towards oscillatory pacemaker activity. In order to achieve this goal, *in silico* analysis was performed (***Figure 7***) because it offers the possibility to visualise all parameters relevant for the system. In every monolayer, we selected a single point from the centre of the illuminated region of the tissue and looked at its dynamic behaviour in phase space.

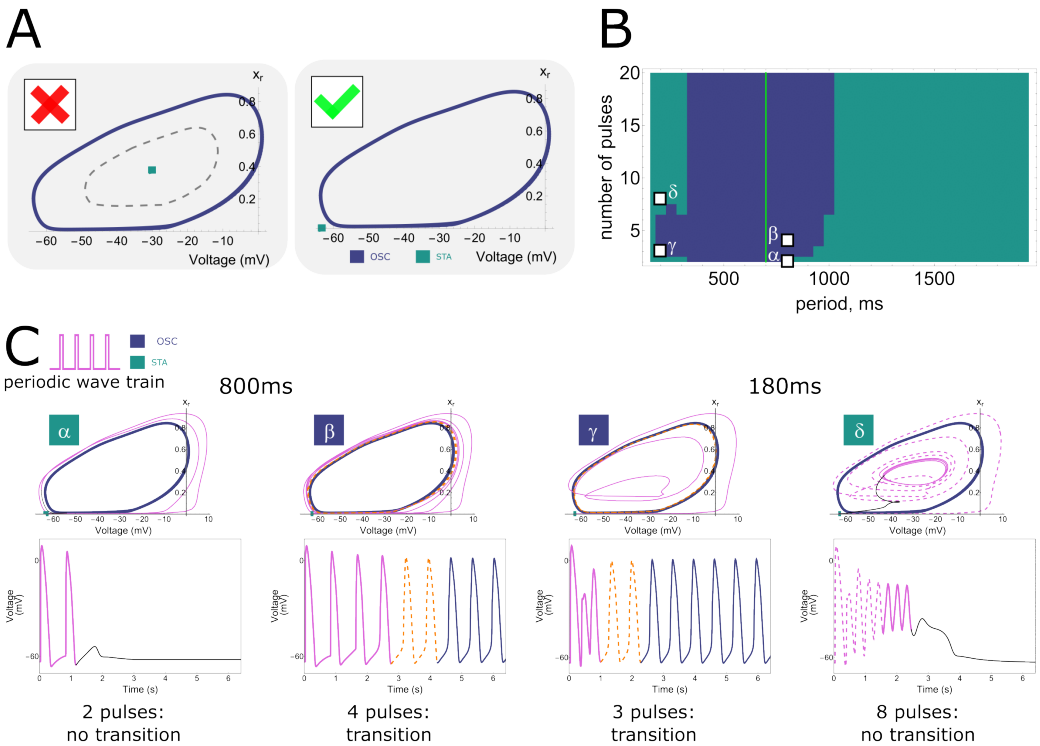

Figure 7. Phase plane projections of pulse-dependent collective state transitions. (A) Phase space trajectories of the NRVM computational model show a limit cycle (OSC) that is not lying around a stable fixed point (STA). **(B)** Parameter space slice showing the relationship between stimulation period and number of pulses for a fixed illumination intensity (1.72 mW/mm^2) and size of the illuminated area (67 pixels edge length). Letters correspond to the graphs shown in **C**. **(C)** Phase space trajectories for different combinations of stimulus train period and number of pulses. A low stimulus frequency (800-ms period) and a low number of pulses (2), as well as a high stimulus frequency (180-ms period) with a high number of pulses (8) do not result in a transition from the resting state to ectopic pacemaker activity, as under these circumstances the system moves towards the stationary stable fixed point from outside and inside the stable limit cycle, respectively. However, at a low stimulation frequency with a high pulse number (4), and at a high stimulation frequency and a low pulse number (3), the stable limit cycle is approached from outside and inside, respectively, and ectopic pacemaker activity is induced.

As was shown in all figures from ***Figure 2*** to ***Figure 6***, illuminated cells do not show dampening oscillations when reaching the stationary state after a transition from the oscillatory state. This behaviour is justified when looking at a projection of the phase space of the model where the voltage V and the gating variable x_r for the rapid delayed outward rectifier K^+ current were chosen for the x- and y-axis, respectively (***Figure 7***A). The stable fixed point (STA) is not located inside the stable limit cycle (OSC) (right panel), hence showing no Hopf bifurcation (left panel) with its associated damped oscillations. The two attractor regions (STA and OSC) were also reconstructed from experimental data and showed two distinct trajectories (***Appendix 2 Figure 6***).

Since we are dealing with a high-dimensional phase space in the *in silico* model, the visualisation of trajectories in time and the corresponding dynamic behaviour is rather complex. However, from the two-dimensional projections onto the V and x_r variables, we can see what causes the frequency and pulse dependency (***Figure 2***, ***Figure 3*** and ***Figure 4***) of ectopic pacemaker activity initiation, as visualised in ***Figure 7***C. Four different pairs of stimulation period and number of pulses were selected, corresponding to different behaviour areas in the parameter space slice for a fixed illumination intensity (1.72 mW/mm^2) and size of the illuminated area (67 pixels edge length) (***Figure 7***B). The first point (α) comes from the region that shows no transition towards collective pace-

maker activity for a low number of pulses (2) and intermediate stimulation periods of 800 ms. The phase space projection (***Figure 7***C) shows that the pulses cycle around the stable limit cycle, and return back to the stable fixed point, indicating that two pulses are not enough to move within the attractor zone of the stable limit cycle. When the number of pulses is increased to 4 (β), the attractor zone of the stable limit cycle is reached from the outside, and collective ectopic pacemaker activity is induced. After switching to a faster stimulation period of 250 ms and sticking to just 3 pulses (γ), the phase space trajectories end up inside the stable limit cycle, but still within the attractor zone. Hence, also this time collective pacemaker activity was induced. If we now increase the number of pulses again, this time to 8 (δ), we are inside the stable limit cycle, but move again out of the region of attraction. Instead of resulting in oscillations, the system moves back to the stationary state through other dimensions by the electrotonic current.

Thus, there is frequency selectivity due to the region of attraction of the stable limit cycle, where too low and too high frequencies result in stationary behaviour. Also pulse accumulation is shown, where more pulses move the system closer to the attractor region. However, we are not dealing with a Hopf bifurcation, because otherwise we would not get back to the stationary state when the number of pulses is increased too much.

Insight into the termination of ectopic pacemaker activity

Let us look once more at a cell inside the illuminated tissue undergoing a stimulus train with a short period of 180 ms from outside and extract all time-dependent variables. In response to a high number of stimuli (17 pulses), the time trace in the phase-space projection plot goes inside the limit cycle (***Figure 8***A) towards a quasi-steady-state, and returns back to the stationary state through a strangely curved line (black). This quasi-steady-state is hidden within the oscillatory trajectory and no pacemaker activity is initiated. When the number of pulses is increased from 17 to 37, the voltage trace shows exactly the same behaviour, indicating that the number of pulses has no influence on the mechanism that moves the tissue back to the stationary state (***Figure 8***B). However, repolarisation reserve does have an influence and makes the transition longer (***Appendix 2 Figure 7***). This can be observed by either moving closer to the boundary of the illuminated region where there is a stronger diffusion/electrotonic influence from the non-illuminated region, or by introducing ionic changes.

To understand what is going on, we studied single cell dynamics under illumination. We already know from ***Figure 6*** that we are dealing with a purely collective phenomenon. Therefore, the single cell dynamics itself showed nothing peculiar, i.e. a standard current-voltage relationship (IV) curve with a single stable equilibrium (not shown). To add a multicellular component to our single cell model we introduced a current that replicates the effect of cell coupling and its associated diffusion. This so-called bias current equals the average in time and space of the current inside the illuminated region using wave trains with a period of 180 ms (the current produced during the quasi-steady-state in ***Figure 8***B). When this bias current is present, the IV curve of the single cell displays two stable equilibria and shows bi-stability (***Figure 8***C-1). The second stable equilibrium cannot be reached with a single pulse, but needs a stimulus train and can only be reached with short stimulation periods (180 ms) and intermediate stimulation amplitudes (-20 mV) (***Figure 8***C-2).

Building on this result, we next applied global stimuli with a period of 180 ms and amplitudes 58, -20, and 50 mV to a virtual cardiomyocyte monolayer with an illuminated square in the center (***Figure 8***D). These pulses were applied when the tissue was either in the oscillatory state (top two rows) or the stationary state (bottom two rows). The stimulus amplitude of -20 mV that was necessary to get the single cell with a bias current into the second stable equilibrium, also terminates oscillatory behaviour (***Figure 8***D-2) while the other two amplitudes of -58 and 50 mV (***Figure 8***D-1,3) don't alter the behaviour of the tissue. However, when starting from the stationary state, the behaviour is opposite and the intermediate amplitude of -20 mV fails to induce collective oscillatory behaviour while the other two amplitudes do elicit this behaviour. We thus conclude that high stimulation frequencies and intermediate stimulus amplitudes are capable of terminating collec-

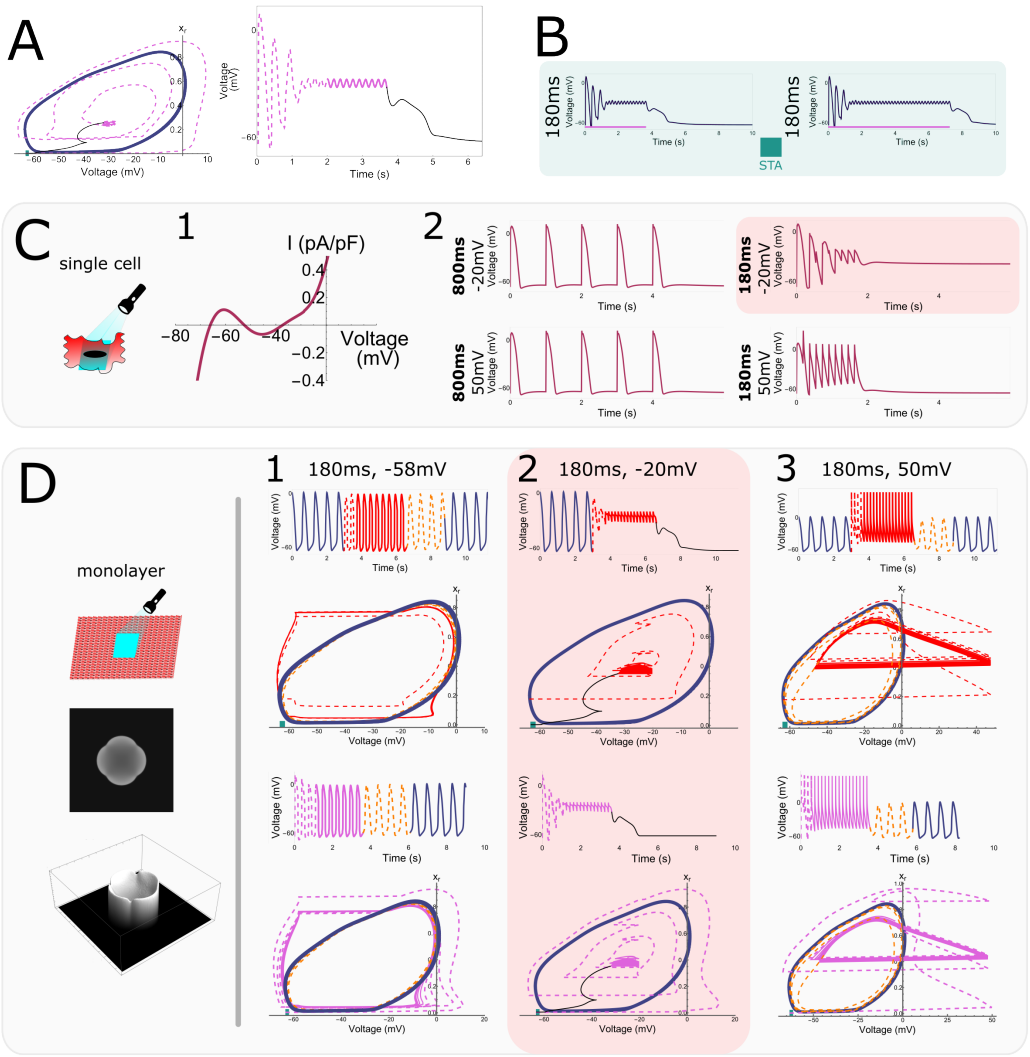

Figure 8. Single cell "hidden" bi-stability and its relation to high frequency pacing. (A) Phase space trajectory and corresponding voltage trace at short pacing period (180 ms). **(B)** Formation of the quasi-steady-state in the center of an irradiated region during a train of 17 and 37 high frequency (180-ms period) pulses. **(C)** Single cell bi-stability. (1) Single cell IV curve for an for illuminated cell (1.72 mW/mm^2) subject to a bias current. (2) Membrane voltage traces for stimulation periods of 1000 and 180 ms and stimulation amplitudes of -20 and 50 mV. A transition to the depolarised stable state occurred for short stimulation periods and low stimulation amplitudes. **(D)** Effect of spatially uniform voltage perturbations of different amplitudes (-58, -20, and 50 mV) and a period of 180 ms in cardiomyocyte monolayers. The top trace and phase space projection show the effect of perturbations when oscillation is ongoing, while the bottom ones show how perturbations affect the tissue is in the stationary resting state. At an amplitude of -20 mV (2) oscillations were terminated when ongoing and could not be initiated when the tissue was in the resting state. In the other two cases (1,3), the opposite happened.

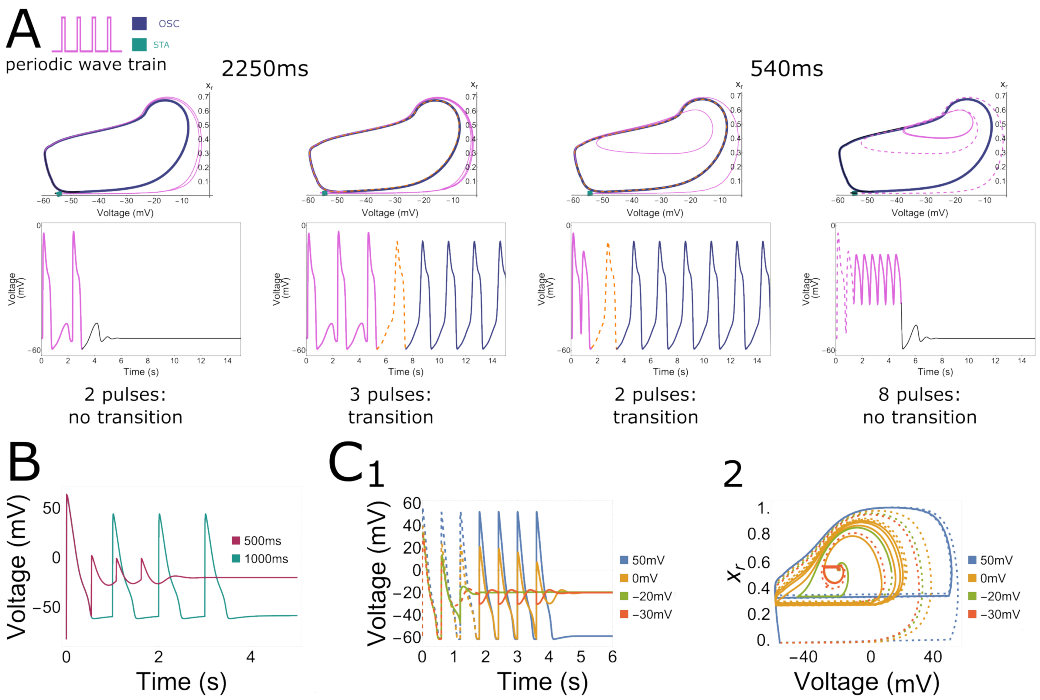

Figure 9. Collective pacemaker activity in a simplified *in silico* NRVM model. (A) Phase space trajectories of a point inside the illuminated region for different combinations of stimulus train period and number of pulses. A low stimulus frequency (2250-ms period) and a low number of 2 pulses, as well as a high stimulus frequency (540-ms period) with a high number of 8 pulses both result in no transition from the resting state to ectopic pacemaker activity, moving towards the stationary stable fixed point from outside and inside the stable limit cycle, respectively. However, when applying 3 pulses with a low frequency (2250-ms period) or 2 pulses with a high frequency (540-ms period), ectopic pacemaker activity is induced and the stable limit cycle is approached from outside and inside, respectively. **(B)** Under illumination, long period stimulation (1000 ms) shows a repolarised state after pacing, while short period stimulation shows a depolarised state (500 ms). **(C) 1** Evolution of the voltage variable as a result of high frequency voltage perturbations of high (blue trajectories) and low (green, orange and red) magnitudes. The dashed parts of graphs demonstrate the transient non-periodic parts of the trajectories, the solid lines show the periodic and stationary states. **2** Corresponding trajectories in the (V, x_r) phase plane.

tive oscillatory behaviour by transitioning through a quasi-steady-state.

We call this kind of bi-stability capable of terminating collective oscillatory behaviour "*hidden bi-stability*" for two reasons: (1) Single cell bi-stability depends on electronic interactions. Hence it can be said that this bi-stability is "hidden" and only emerges in collective behaviour. (2) It's possible to escape the region of attraction of the oscillatory trajectory through opposite paths.

It's complex, but not as complex as it seems

While it may be believed that the observed phenomena and explanations are intrinsic to entangled interactions specific to the complexity of a biological sample (*in vitro*) and a realistic computational model (*in silico*), we show here that this is not the case. By reducing the model equations, we show that collective oscillatory behaviour is not limited to the specific case of NRVMs. We started from the initial NRVM equations and reduced them to contain only a single depolarising current (I_{Na}), two repolarising currents (I_{Kr} and the time-independent I_{K1}), and a spatially dependent optogenetic current (I_{ChR2}). Fast variables in these currents were assumed to keep their steady-state value, which caused them to be time-independent. The exact equations can be found in ***Appendix 1***.

Using this simplified system of three variables (the voltage V, the closing gate of the Na^+ channel h, and the opening gate of the K^+ channel x_r), we were able to reproduce all key features

(frequency selectivity, pulse accumulation and bi-stability) of the more complex systems (***Figure 9***).

Just like in ***Figure 7***C, the simplified model showed no initiation of collective pacemaker activity at a low number of 2 pulses and a low stimulation frequency of 2250 ms or at a high number of 8 pulses and a high stimulation frequency of 540 ms (***Figure 9***A). However, pacemaker activity was induced when applying 3 pulses and a low stimulation frequency or 2 pulses and a high stimulation frequency. At a low frequency, the phase space projection (again projected onto the V and x_r variable plane) shows that the limit cycle is approached from the outside, while at high frequencies it is approached from the inside. Altogether, these results show frequency selectivity and pulse accumulation in the simplified model (***Figure 9***A). To explain the findings in the rightmost panel of ***Figure 9***A, we had a closer look at the single cell dynamics under high stimulation frequencies. As shown in ***Figure 9***B, 4 pulses at a low frequency (1000-ms period) resulted in normal behaviour, but high frequency stimulation (500-ms period) pushed the cell towards a stably elevated membrane potential (***Figure 9***B). Looking at the influence of stimulus amplitude on the ability to get to this elevated membrane potential, it appears that after 7 pulses 3 of the 4 traces move towards the elevated membrane potential of -20 mV (***Figure 9***C). Panels B and C combined give us the same qualitative behaviour as seen in ***Figure 8***C. The qualitative behaviours of ***Figure 4***A and ***Figure 8***D were also reproduced and can be found in ***Appendix 2 Figure 8***.

Discussion

In this study, *in vitro* observations were combined with *in silico* modelling to study and gain mechanistic insight into collective electrophysiological behaviour in NRVM monolayers.

- Firstly, we demonstrated the existence of transitions from stationary cardiac monolayers towards ones that show pacemaker activity coming from an illuminated region, which are induced by wave trains of external pulses (***Figure 1***) as a manifestation of **collective bi-stability**. This transition between the two states is dependent on four variables: the light intensity applied to the illuminated region, the size of the illuminated region, the number of pulses of an incoming wave-train, and the frequency of the pulses of the incoming wave train (***Figure 2***, ***Figure 3***, ***Figure 5*** and ***Appendix 2 Figure 4***, ***Figure 5***). *In vitro* experiments were quantitatively reproduced *in silico*, thereby establishing a link between model and experiment (***Figure 4***, ***Figure 5*** and ***Appendix 2 Figure 4***, ***Figure 5***)).
- Secondly, we studied the mechanisms underlying the initiation and termination of pacemaker activity. In the presence of a diffusion current (or bias current in the case of a single cell), the illuminated cells transition to a second equilibrium under high frequency pacing. Because this second equilibrium only appears in a coupled system (or in the presence of a bias current), we can also speak of a **hidden bi-stability**. Hence, hidden bi-stability (high vs. low stationary resting membrane) is shown to underlie the collective phenomena (stationary vs. oscillatory behaviour) (***Figure 6 Figure 7 Figure 8***, ***Appendix 2 Figure 6*** and ***Appendix 2 Figure 7***).

Below, we compare these phenomena to different types of arrhythmic events and mechanisms of bi-stability in cardiac tissue, and extend the relevance of our mechanisms to spiking behaviour in neuronal and other biophysical systems.

Ectopic pacemaker activity in cardiology

The generation of ectopic beats is considered as one of the main mechanisms triggering and maintaining cardiac arrhythmias (***Pogwizd et al.*** (***1992***)). In most cases, ectopic sources are believed to be a result of triggered activity, which can manifest itself as early afterdepolarizations (EADs) or delayed afterdepolarizations (DADs) (***Qu et al.*** (***2014***)). Such ectopic sources are typically initiated by high frequency pacing resulting in a Ca^{2+} overload that triggers EADs and DADs (***Lerman et al.*** (***2024***)). However, as we didn't observe Ca^{2+} overload, the phenomenon observed in this study resembles induced pacemaker activity instead. In contrast with ectopy, this pacemaker activity is initiated at low pacing frequencies. Therefore our findings might explain the phenomenon of

bradycardia-induced triggered activity (***Brachmann et al.*** (***1983***)). The initiation of oscillations in our monolayers is the result of the spatial dynamics of the system, which stands in contrast with the frequency dependency of EADs that can be explained on a single cell level (***Tran et al.*** (***2009***); ***Qu et al.*** (***2014***)). Our optogenetic current is absent in normal cardiac tissue, but its associated depolarisation could be caused by other late activating inward currents, which are also essential in the induction of EADs or DADs (***Song et al.*** (***2008***); ***Qu et al.*** (***2014***)): e.g. the late Na current ($I_{Na,L}$, ***Belardinelli et al.*** (***2015***)), reactivation of I_{CaL} (***Tran et al.*** (***2009***)), or NCX activity (***Song et al.*** (***2015***)). In addition, collective bi-stability might be observed in the presence of oxidative stress, ischemia or chronic heart failure (***Belardinelli et al.*** (***2015***); ***Shryock et al.*** (***2013***); ***Undrovinas et al.*** (***1999***)), where there is depolarisation-induced automaticity (triggered activity) caused by a background current (e.g. $I_{Na,L}$).

The ectopic pacemaker activity in this study is a direct result of the combination of single cell depolarisation with spatial effects. Due to the additional inward current produced by the activation of CheRiff, a single uncoupled illuminated cell goes to a steady depolarised state (***Figure 6***B). However, in a multicellular environment there is a repolarising electrotonic coupling current working against this depolarising light-induced current. This repolarising current is a consequence of the interaction between depolarised and non-depolarised parts in the monolayer. By playing with the illumination intensity and the size of the illuminated region, we were able to balance these de- and re-polarising effects to create a bi-stable regime (STA vs. OSC). This also explains why there are no oscillations present in the center of a large illuminated region, since there the electrotonic current is lower than at its edges. (***Figure 6***C). On the other hand, if the electrotonic current is too strong, it will prevent depolarisation by the optogenetic current and, as a consequence, the system wil stay in the stationary state. The balancing of currents also explains why the oscillatory boundary moves closer to the edge of the illuminated region at higher light intensities, since under those circumstances the depolarising current will overpower the spatial effects. However, when the illumination is very strong, it is possible to have oscillations that don't need to be induced (***Figure 1***B) and can even come from the corners of the illuminated region (***Appendix 2 Figure 3***, ***Teplenin et al.*** (***2018***)). This last-mentioned phenomenon appears because the curvature of the boundary between illuminated and not-illuminated regions influences the electrotonic current.

Interplay between microscopic (single cell) and macroscopic (monolayer) behaviour

Collective bi-stability, as described in the previous section, is a bi-stability between two distinct behaviours (stationary STA and oscillatory OSC behaviour) that occur at the macroscopic level (monolayer). However, by looking more deeply at the dynamics that happen at the microscopic level (single cell), we can get more insight into the underlying mechanism(s). At the single cell level, the dynamic transition between a stationary monolayer and one showing induced pacemaker activity relies on two main processes:

1. For the initiation of pacemaker activity, pulse accumulation (at intermediate frequencies) is necessary to bring the system into the attracting region of the oscillatory state.
2. For the termination of pacemaker activity, an interaction takes place between "hidden" bi-stable dynamics and coupling currents at high frequencies.

Both these processes occur as a consequence of wave pulses outside of the illuminated region. At low frequencies, no oscillatory activity can be induced. At intermediate frequencies, it is possible to escape the attracting zone of the stationary state and cross the separatrix into the attracting zone of the oscillatory state. However, for even higher frequencies, the system gets pushed out of the attracting zone of the oscillatory state again and through hidden bi-stability it returns to the stationary state.

Our data on the termination mechanism of induced pacemaker activity (***Figure 8***) indicate that we are not dealing with classical STA-OSC bi-stability (***Winfree*** (***2001***)). In systems displaying classical bi-stability between a limit cycle and the resting state, pacemaker annihilation can be achieved

by applying sufficiently high frequency voltage perturbations. Through pulse accumulation it is then possible to exit the basin of attraction in the reverse direction from which it was entered. In contrast, our system enters (from outside the limit cycle) and leaves (towards the inside of the limit cycle) the attraction zone in opposite directions. This was concluded from the absence of a Hopf bifurcation in our system (***Figure 7***).

The seemingly fragile nature of hidden bi-stability might be a requirement for coexistence of excitable (non-illuminated) and bi-stable (illuminated) regimes. Otherwise, if the hills and dips of the N-shaped steady-state IV curve are large (***Figure 8***C-1), they would be in the same range as the big currents of fast ion channels, thereby preventing the subtle interaction between the large ionic cell currents and small repolarising coupling currents.

Although the termination mechanism was shown to be amplitude-dependent (***Figure 8***C-D), the appropriate perturbation amplitudes are "automatically" selected by a high frequency train of travelling waves of excitation without any *a priori* knowledge about the state of the system. This wave train terminated ectopic triggers (***Figure 2***), which is in accordance with previous publications (***Moak and Rosen*** (***1984***); ***Glikson et al.*** (***2021***)). These publications also showed that uniform high voltage shocks are unable to terminate ectopic sustained activity, similar to our findings (***Figure 8***).

Although its manifestations are clear in a monolayer system, hidden bi-stability might be challenging to be observed in single cell patch-clamp experiments. In ***Figure 8***C-1, the height of dips and hills of the N-shaped steady-state IV curve under bias current are $\approx 0.2pA/pF$. While it is possible to perform patch-clamping on individual cells in a monolayer experiencing diffusion currents, measurements of small amplitudes can be hindered by the statistical and instrumental errors of voltage-clamp recordings. The voltage bi-stability we are looking for can, for example, easily be lost via a shift in current balance due to the non-zero resistance of the patch pipette in current clamp mode. This might explain why the phenomenon of hidden bi-stability has only rarely been reported, for example in an *in silico* study dedicated to myotony in muscle fibres (***Cannon et al.*** (***1993***)).

Extrapolation and translation

All key aspects of the initiation and termination of induced pacemaker activity, i.e. the points itemized above, were also demonstrated in a simplified 3 variable reaction-diffusion model (***Figure 9***, ***Appendix 2 Figure 8***), implicating the more general nature of this observed phenomenon. A rigorous mathematical analysis can be accomplished in future work, but might be challenging due to the lack of efficient analytical tools to describe fully developed limit cycle oscillations in reaction-diffusion systems (***Sherratt and Smith*** (***2008***)). Based on the reproduction of our results in such a simplified model, we showed that we don't need the full complexity of an ionic cardiomyocyte model, enabling extrapolation and translation of our results towards other scientific disciplines.

Frequency-dependent initiation and termination of oscillatory activity is not exclusive to cardiac systems, but is well known in a variety of non-linear biophysical systems. For example, the actomyosin cortex in the social amoeba *Dictyostelium discoideum* responds to short pulses of 3',5'-cyclic adenosine monophosphate (cAMP) by damped oscillations in average actin content, thereby allowing fine time-selective responses to either internal (pseudopodia initiation) or external (cAMP release) perturbations (***Westendorf et al.*** (***2013***)). Moreover, in synthetic gene regulatory networks, subthreshold stimuli might be used to discriminate environmental stimuli (e.g. growth factor release, heat shock) (***Guantes and Poyatos*** (***2006***)). Also neurons can differentiate external stimuli depending on their frequency. As mentioned in the introduction, the frequency-dependent initiation and termination of oscillatory activity is known as '*resonance*' in neuroscience. It is interesting to compare the resonance properties of our system with those actively studied in neurons.

Resonant neurons, also known as resonate-and-fire neurons or type II excitability neurons (***Izhikevich*** (***2000***)), are governed by sub-threshold oscillations initiated due to proximity of the resting state to a Hopf bifurcation (***Hutcheon and Yarom*** (***2000***); ***Roach et al.*** (***2018***)). They react to a stimulus train as follows: The first pulse initiates a damped sub-threshold oscillation of the

membrane potential, while the effect of the second pulse depends on its timing. If timed correctly, it adds to the first pulse and either increases the amplitude of the sub-threshold oscillation or evokes repetitive spiking (transition to a limit cycle). Thus, the response and spiking of the resonator neuron depends on the frequency content of the input. These types of spiking neurons are usually associated with Bogdanov-Takens bifurcations (***Izhikevich*** (***2000***)). However, another type of bifurcation, a saddle-node-loop (SNL) bifurcation, is also capable of generating spiking neurons and allows a bi-stability regime, in which the stable state lies outside the limit cycle similar to our case (***Figure 7***).

SNL bifurcations were previously identified in neurons (***Hesse et al.*** (***2017***); ***Hesse and Schreiber*** (***2019***); ***Schleimer et al.*** (***2021***)), in a model of transcriptional regulation of the cell (***Ciliberto et al.*** (***2005***)), and in the design of combined genetic switches (***Perez-Carrasco et al.*** (***2018***)). Our result might represent the emergent analogue of a SNL bifurcation with resonant transitions on a neuronal/non-linear network level. SNL bifurcations have already been identified in the networks of coupled Kuramoto limit cycle oscillators both in a broad (***Martens et al.*** (***2009***); ***Childs and Strogatz*** (***2008***)) and in a neuroscience context (***Buendía et al.*** (***2021***)). In these studies, SNL bifurcations were identified using dimensionality reduction techniques while ignoring the whole wealth of transient and finite-size phenomena. Moreover the Kuramoto model is a model without many physical details, describing a weak forcing regime on an idealized limit cycle oscillator, in which oscillations cannot be destroyed but only phase shifted. In our case, we provide a more realistic biophysically motivated model, which allows a strong forcing regime and destruction of oscillations due to the phenomenon of hidden bi-stability. This gives us reason to believe that idealized Kuramoto models could possess resonant properties if augmented/modified with sufficient physical/biophysical details. SNL bifurcations and hidden bi-stability could also be studied in a range of other unexplored biophysical situations including high frequency stimulation for the termination of neuronal oscillations during Parkinson disease (***Touboul et al.*** (***2020***)), multi compartment cable computational models of the neuron (***Schwemmer and Lewis*** (***2012***)), and bi-stability in neurons *in vitro* (***Le et al.*** (***2006***)). Additional studies can be carried out in neuroscience by local optogenetic activation of depolarizing ion channels, both *in vivo* ***Lu et al.*** (***2015***) and *in silico* in non-local models ***Selvaraj et al.*** (***2015***); ***Heitmann et al.*** (***2017***).

Conclusion

Using both *in vitro* and *in silico* models, we explored a mechanism for frequency-dependent initiation and termination of oscillatory activity (i.e. induced pacemaker activity) in non-homogeneous cardiac tissue. This mechanism could be extended to more general excitable systems and is in neuroscience also known under the term resonance. Our collective "resonance" mechanism could be used to study or control collective states in cardiac but also other excitable systems.

Materials and Methods

Preparation of monolayers of NRVMs expressing the light-activatable cation channel CheRiff

All animal experiments were reviewed and approved by the Animal Experiments Committee of the Leiden University Medical Center and carried out in accordance with Directive 2010/63/EU of the European Union on the protection of animals used for scientific purposes.. Monolayers of NRVMs were established as previously described ***Engels et al.*** (***2015***). Briefly, the hearts were excised from anaesthetised 2-day-old Wistar rats. The ventricles were cut into small pieces and dissociated in a solution containing $450\ \mathrm{U/ml}$ collagenase type I (Worthington, Lakewood, NJ) and 18,75 Kunitz/ml DNase I (Sigma-Aldrich, St. Louis, MO). The resulting cell suspension was enriched for cardiomyocytes by preplating for 120 minutes in a humidified incubator at $37°$C and 5% CO_2 using Primaria culture dishes (Becton Dickinson, Breda, the Netherlands). Finally, the cells were seeded on round glass coverslips ($d = 15\ \mathrm{mm}$; Gerhard Menzel, Braunschweig, Germany) coated

with bovine fibronectin (100 μg/ml; Sigma-Aldrich) to establish confluent monolayers. After incubation overnight in an atmosphere of humidified 95% air- 5% CO_2 at 37°C, these monolayers were treated with Mitomycin-C (10 μg/ml; Sigma-Aldrich) for 2 hours to minimise proliferation of the non-cardiomyocytes. At day 4 of culture, the NRVM monolayers were incubated for 20-24 h with lentiviral vector particles encoding CheRiff (***Hochbaum et al.*** (***2014***)), a light-gated depolarising ion channel of the channelrhodopsin family (***Wang et al.*** (***2015***)), at a dose resulting in homogeneous transduction of nearly 100% of the cells (***Feola et al.*** (***2017***); ***Ördög et al.*** (***2023***)). Next, the cultures were washed once with phosphate-buffer saline, given fresh culture medium and kept under culture conditions for 3-4 additional days.

Optical voltage mapping and patterned illumination of NRVM monolayers

After 8-10 days of culturing, NRVM monolayers were optically mapped using the voltage-sensitive dye di-4-ANBDQBS (52.5 μM final concentration; ITK diagnostics, Uithoorn, the Netherlands) as reported previously (***Feola et al.*** (***2017***)). The mapping setup (***Appendix 2 Figure 1***) was based on a 100 × 100 pixel CMOS Ultima-L camera (Scimedia, Costa Mesa, CA). The field of view was 16 × 16 mm resulting in a spatial resolution of 160 μm/pixel. For targeted illumination of monolayers the setup was optically conjugated to a digitally controlled micro-mirror device (DMD), the Polygon 400 (Mightex Systems, Toronto, ON), with a high power blue (470 nm) LED (BLS-LCS-0470-50-22-H, Mightex Systems). Before starting the actual experiments, all monolayers were mapped during 1-Hz electrical point stimulation to check baseline conditions. Electrical stimulation was performed by applying 10-ms-long rectangular electrical pulses with an amplitude of 8 V to a bipolar platinum electrode with a spacing of 1.5 mm between anode and cathode. Only cultures with an action potential duration (APD) at 80% repolarization (APD_{80}) below 350 ms and a conduction velocity (CV) above 18 cm/s were used for further experiments. Stimuli were applied in trains that varied in number and period. Whenever the outcome was reproducible three consecutive times in a single monolayer, it was counted as successful and included as one measurement in the total dataset. The constant light intensity was varied in the range of (0.03125-0.25 mW/mm^2) to search the critical value for the bi-stable regime. For experiments in which the light intensity was varied the rectangular-shaped area of illumination was in the range of 4×4 to 6×6 mm. The highest achievable irradiation intensity (0.3125 mW/mm^2) was used to perform size modulation experiments. The resulting electrical activity was recorded for 6-24 s at exposure times of 6 ms per frame.

Post-processing of optical mapping data

Data processing was performed using specialized BV Ana software (Scimedia), ImageJ (***Schneider et al.*** (***2012***)) and custom-written scripts in Wolfram Mathematica (Wolfram Research, Hanborough, Oxfordshire, United Kingdom). APD and CV were calculated as described previously (***Feola et al.*** (***2017***)). To prepare representative frames of wave propagation, optical mapping videos were filtered with a spatial averaging filter (3 × 3 stencil) and a derivative filter.

Attractor reconstruction

Multiple attractor reconstruction is based on Takens's embedding theorem (***Takens*** (***1981***)) by plotting phase space trajectories in $(V(t), V(t+\tau))$ coordinates. The optimal time delay τ was determined by calculating the minimum of the autocorrelation function (***Clemson and Stefanovska*** (***2014***)). Linear drift removal was applied before plotting phase space trajectories.

Detailed electrophysiological model

In this study, the Majumder-Korhonen model (***Majumder et al.*** (***2016***)) of NRVM monolayers was used, whose monodomain reaction-diffusion equation is formulated as follows:

$$\frac{\partial V}{\partial t} = \nabla \cdot (D \nabla V) - \frac{I_{ion} + I_{ChR2}(x, y)}{C_m}, \tag{1}$$

where I_{ion} is the sum of all ionic currents, $\mathcal{D}$ is the diffusion coefficient equal to 0.00095 cm^2/ms and $I_{ChR2}(x, y)$ is the spatially controlled optogenetic current. In comparison to the original model, I_{Na} was increased 1.3-fold and, I_{Ca_L} and I_{Kr} were both reduced 0.7-fold. The steady-state voltage dependency for the inactivation variable h of the fast Na$^+$ current was changed to $h_\infty = [1 + e^{\frac{(72+V)}{6.07}}]^{-1}$, where V is the transmembrane potential. The resulting CV was 20 cm/s. The optogenetic current I_{ChR2} was formulated based on the ***Boyle et al.*** (***2013***) I_{ChR2} model with the introduction of rectifying conduction properties and voltage-dependent state transitions (***Williams et al.*** (***2013***)). The irradiation intensity varied in the range of 0.165–0.175 mW/mm^2.

The forward Euler method was used to integrate the equations with a time step $\Delta t = 0.02ms$ and a centered finite-differencing scheme to discretise the Laplacian with a space step of $\Delta x = 0.0625mm$. The total computational domain size was 256 $\times$ 256 grid points; while the centrally irradiated square with the optogenetic current consisted of 80 $\times$ 80 grid points. To create stationary initial conditions, the model was integrated for 2 minutes before a train of stimuli was applied from the upper border of the domain.

Acknowledgements

We would like to thank Desmond Kabus for useful discussions that improved the manuscript and Annemarie Kip and Cindy Bart for the production of the CheRiff-encoding lentiviral vector LV.GgTnnt2.CheRiff eYFP.WHVoPRE.

This work was supported by the European Research Council (ERC consolidator grant 101044831 to DAP) and the Netherlands Organization for Scientific Research (NWO Vidi grant 917143 to DAP and ZonMW Off Road grant 04510012110051 to TDC) .

Author contributions

Conceptualization: AST, AVP, DAP, TDC
Methodology: AST
Software: AST, RM, NNK
Formal analysis: AST, TDC
Investigation: AST
Resources: AAFdV, DAP
Writing—original draft: TDC
Writing—review & editing: AST, AAFdV, AVP, DAP, TDC
Visualization: AST, TDC
Supervision: DAP and TDC
Project administration: DAP
Funding acquisition: DAP, TDC

References

Angeli D, Ferrell Jr JE, Sontag ED. Detection of multistability, bifurcations, and hysteresis in a large class of biological positive-feedback systems. Proceedings of the National Academy of Sciences. 2004; 101(7):1822–1827.

Belardinelli L, Giles WR, Rajamani S, Karagueuzian HS, Shryock JC. Cardiac late Na+ current: Proarrhythmic effects, roles in long QT syndromes, and pathological relationship to CaMKII and oxidative stress. Heart Rhythm. 2015; 12(2):440–448. doi: https://doi.org/10.1016/j.hrthm.2014.11.009.

Boyle PM, Williams JC, Ambrosi CM, Entcheva E, Trayanova NA. A comprehensive multiscale framework for simulating optogenetics in the heart. Nature communications. 2013; 4:2370. doi: 10.1038/ncomms3370.

Brachmann J, Scherlag BJ, Rosenshtraukh LV, Lazzara R. Bradycardia-dependent triggered activity: relevance to drug-induced multiform ventricular tachycardia. Circulation. 1983; 68(4):846–856. doi: 10.1161/01.CIR.68.4.846.

Buendía V, Villegas P, Burioni R, Muñoz MA. Hybrid-type synchronization transitions: Where incipient oscillations, scale-free avalanches, and bistability live together. Phys Rev Research. 2021 Jun; 3:023224. doi: 10.1103/PhysRevResearch.3.023224.

Cannon SC, Brown RH, Corey DP. Theoretical reconstruction of myotonia and paralysis caused by incomplete inactivation of sodium channels. Biophysical Journal. 1993; 65(1):270–288. doi: https://doi.org/10.1016/S0006-3495(93)81045-2.

Childs LM, Strogatz SH. Stability diagram for the forced Kuramoto model. Chaos: An Interdisciplinary Journal of Nonlinear Science. 2008; 18(4):043128. doi: 10.1063/1.3049136.

Ciliberto A, Novak B, Tyson JJ. Steady States and Oscillations in the p53/Mdm2 Network. Cell Cycle. 2005; 4(3):488–493. doi: 10.4161/cc.4.3.1548.

Clemson PT, Stefanovska A. Discerning non-autonomous dynamics. Physics Reports. 2014; 542(4):297–368. doi: https://doi.org/10.1016/j.physrep.2014.04.001, discerning non-autonomous dynamics.

Dana SK, Roy PK, Kurths J. Complex dynamics in physiological systems: From heart to brain. Springer Science & Business Media; 2008.

Engels MC, Askar SF, Jangsangthong W, Bingen BO, Feola I, Liu J, Majumder R, Versteegh MI, Braun J, Klautz RJ, et al. Forced fusion of human ventricular scar cells with cardiomyocytes suppresses arrhythmogenicity in a co-culture model. Cardiovascular research. 2015; 107(4):601–612.

Feola I, Volkers L, Majumder R, Teplenin A, Schalij MJ, Panfilov AV, de Vries AAF, Pijnappels DA. Localized Optogenetic Targeting of Rotors in Atrial Cardiomyocyte Monolayers. Circulation: Arrhythmia and Electrophysiology. 2017; 10(11):e005591. doi: 10.1161/CIRCEP.117.005591.

Glikson M, Nielsen JC, Kronborg MB, Michowitz Y, Auricchio A, Barbash IM, Barrabes JA, Boriani G, Braunschweig F, Brignole M, et al. 2021 ESC Guidelines on cardiac pacing and cardiac resynchronization therapy developed by the Task Force on cardiac pacing and cardiac resynchronization therapy of the European Society of Cardiology (ESC) with the special contribution of the European Heart Rhythm Association (EHRA). European Heart Journal. 2021; 42(35):3427–3520.

Guantes R, Poyatos JF. Dynamical Principles of Two-Component Genetic Oscillators. PLOS Computational Biology. 2006 03; 2(3):1–10. doi: 10.1371/journal.pcbi.0020030.

Guevara MR. Bifurcations Involving Fixed Points and Limit Cycles in Biological Systems. In: Nonlinear Dynamics in Physiology and Medicine New York, NY: Springer New York; 2003. p. 41–85. doi: 10.1007/978-0-387-21640-9_3.

Heitmann S, Rule M, Truccolo W, Ermentrout B. Optogenetic Stimulation Shifts the Excitability of Cerebral Cortex from Type I to Type II: Oscillation Onset and Wave Propagation. PLOS Computational Biology. 2017 01; 13(1):1–13. doi: 10.1371/journal.pcbi.1005349.

Hesse J, Schleimer JH, Schreiber S. Qualitative changes in phase-response curve and synchronization at the saddle-node-loop bifurcation. Phys Rev E. 2017 May; 95:052203. doi: 10.1103/PhysRevE.95.052203.

Hesse J, Schreiber S. How to correctly quantify neuronal phase-response curves from noisy recordings. Journal of computational neuroscience. 2019; 47(1):17–30. doi: 10.1007/s10827-019-00719-3.

Hochbaum DR, Zhao Y, Farhi SL, Klapoetke N, Werley CA, Kapoor V, Zou P, Kralj JM, Maclaurin D, Smedemark-Margulies N, et al. All-optical electrophysiology in mammalian neurons using engineered microbial rhodopsins. Nature methods. 2014; 11(8):825–833. doi: 10.1038/nmeth.3000.

Hutcheon B, Yarom Y. Resonance, oscillation and the intrinsic frequency preferences of neurons. Trends in Neurosciences. 2000; 23(5):216–222. doi: https://doi.org/10.1016/S0166-2236(00)01547-2.

Izhikevich EM. Neural Excitability, Spiking and Bursting. International Journal of Bifurcation and Chaos. 2000; 10(06):1171–1266. doi: 10.1142/S0218127400000840.

Jangsangthong W, Feola I, Teplenin A, Schalij M, Ypey D, De Vries A, Pijnappels D. 29-03: Optogenetically-induced microfoci of oxidative stress increase pro-arrhythmic risk. EP Europace. 2016 06; 18(suppl_1):i27–i27. doi: 10.1093/europace/18.suppl_1.i27b.

Le T, Verley DR, Goaillard JM, Messinger DI, Christie AE, Birmingham JT. Bistable behavior originating in the axon of a crustacean motor neuron. Journal of neurophysiology. 2006; 95(3):1356–1368. doi: 10.1152/jn.00893.2005.

Lerman BB, Markowitz SM, Cheung JW, Thomas G, Ip JE. Ventricular Tachycardia Due to Triggered Activity: Role of Early and Delayed Afterdepolarizations. Clinical Electrophysiology. 2024; 10(2):379–401.

Lu Y, Truccolo W, Wagner FB, Vargas-Irwin CE, Ozden I, Zimmermann JB, May T, Agha NS, Wang J, Nurmikko AV. Optogenetically induced spatiotemporal gamma oscillations and neuronal spiking activity in primate motor cortex. Journal of neurophysiology. 2015; 113(10):3574–3587.

Majumder R, Engels MC, de Vries AA, Panfilov AV, Pijnappels DA. Islands of spatially discordant APD alternans underlie arrhythmogenesis by promoting electrotonic dyssynchrony in models of fibrotic rat ventricular myocardium. Scientific reports. 2016; 6. doi: 10.1038/srep24334.

Martens EA, Barreto E, Strogatz SH, Ott E, So P, Antonsen TM. Exact results for the Kuramoto model with a bimodal frequency distribution. Phys Rev E. 2009 Feb; 79:026204. doi: 10.1103/PhysRevE.79.026204.

Moak JP, Rosen MR. Induction and termination of triggered activity by pacing in isolated canine Purkinje fibers. Circulation. 1984; 69(1):149–162.

Ördög B, De Coster T, Dekker SO, Bart CI, Zhang J, Boink GJ, Bax WH, Deng S, den Ouden BL, de Vries AA, et al. Opto-electronic feedback control of membrane potential for real-time control of action potentials. Cell Reports Methods. 2023; 3(12).

Ördög B, Teplenin A, De Coster T, Bart CI, Dekker SO, Zhang J, Ypey DL, de Vries AA, Pijnappels DA. The effects of repetitive use and pathological remodeling on channelrhodopsin function in cardiomyocytes. Frontiers in Physiology. 2021; 12:710020.

Perez-Carrasco R, Barnes CP, Schaerli Y, Isalan M, Briscoe J, Page KM. Combining a Toggle Switch and a Repressilator within the AC-DC Circuit Generates Distinct Dynamical Behaviors. Cell Systems. 2018; 6(4):521–530.e3. doi: https://doi.org/10.1016/j.cels.2018.02.008.

Pogwizd SM, Hoyt RH, Saffitz JE, Corr PB, Cox JL, Cain ME. Reentrant and focal mechanisms underlying ventricular tachycardia in the human heart. Circulation. 1992; 86(6):1872–1887. doi: 10.1161/01.CIR.86.6.1872.

Qu Z, Hu G, Garfinkel A, Weiss JN. Nonlinear and stochastic dynamics in the heart. Physics Reports. 2014; 543(2):61–162. doi: https://doi.org/10.1016/j.physrep.2014.05.002.

Roach JP, Pidde A, Katz E, Wu J, Ognjanovski N, Aton SJ, Zochowski MR. Resonance with subthreshold oscillatory drive organizes activity and optimizes learning in neural networks. Proceedings of the National Academy of Sciences. 2018; 115(13):E3017–E3025. doi: 10.1073/pnas.1716933115.

Schleimer JH, Hesse J, Contreras SA, Schreiber S. Firing statistics in the bistable regime of neurons with homoclinic spike generation. Phys Rev E. 2021 Jan; 103:012407. doi: 10.1103/PhysRevE.103.012407.

Schneider CA, Rasband WS, Eliceiri KW. NIH Image to ImageJ: 25 years of image analysis. Nature methods. 2012; 9(7):671–675.

Schwemmer MA, Lewis TJ. Bistability in a Leaky Integrate-and-Fire Neuron with a Passive Dendrite. SIAM Journal on Applied Dynamical Systems. 2012; 11(1):507–539. doi: 10.1137/110847354.

Selvaraj P, Sleigh JW, Kirsch HE, Szeri AJ. Optogenetic induced epileptiform activity in a model human cortex. Springerplus. 2015; 4(1):1–6. doi: 10.1186/s40064-015-0836-7.

Sherratt JA, Smith MJ. Periodic travelling waves in cyclic populations: field studies and reaction-diffusion models. Journal of The Royal Society Interface. 2008; 5(22):483–505. doi: 10.1098/rsif.2007.1327.

Shryock JC, Song Y, Rajamani S, Antzelevitch C, Belardinelli L. The arrhythmogenic consequences of increasing late INa in the cardiomyocyte. Cardiovascular Research. 2013 06; 99(4):600–611. doi: 10.1093/cvr/cvt145.

Song Y, Shryock JC, Belardinelli L. An increase of late sodium current induces delayed afterdepolarizations and sustained triggered activity in atrial myocytes. American Journal of Physiology-Heart and Circulatory Physiology. 2008; 294(5):H2031–H2039. doi: 10.1152/ajpheart.01357.2007, pMID: 18310511.

Song Z, Ko C, Nivala M, Weiss J, Qu Z. Calcium-Voltage Coupling in the Genesis of Early and Delayed Afterdepolarizations in Cardiac Myocytes. Biophysical Journal. 2015; 108(8):1908–1921. doi: https://doi.org/10.1016/j.bpj.2015.03.011.

Takens F. Detecting strange attractors in turbulence. In: Dynamical Systems and Turbulence, Warwick 1980 Berlin, Heidelberg: Springer Berlin Heidelberg; 1981. p. 366–381. doi: 10.1007/BFb0091924.

Tan P, He L, Huang Y, Zhou Y. Optophysiology: Illuminating cell physiology with optogenetics. Physiological reviews. 2022; 102(3):1263–1325.

Teplenin AS, Dierckx H, de Vries AAF, Pijnappels DA, Panfilov AV. Paradoxical Onset of Arrhythmic Waves from Depolarized Areas in Cardiac Tissue Due to Curvature-Dependent Instability. Phys Rev X. 2018 Jun; 8:021077. doi: 10.1103/PhysRevX.8.021077.

Touboul JD, Piette C, Venance L, Ermentrout GB. Noise-Induced Synchronization and Antiresonance in Interacting Excitable Systems: Applications to Deep Brain Stimulation in Parkinson's Disease. Phys Rev X. 2020 Mar; 10:011073. doi: 10.1103/PhysRevX.10.011073.

Tran D, Sato D, Yochelis A, Weiss J, Garfinkel A, Qu Z. Bifurcation and Chaos in a Model of Cardiac Early Afterdepolarizations. Physical Review Letters. 2009 jun; 102(25):258103. doi: 10.1103/PhysRevLett.102.258103.

Undrovinas A, Maltsev V, Sabbah H. Repolarization abnormalities in cardiomyocytes of dogs with chronic heart failure: role of sustained inward current. Cellular and Molecular Life Sciences CMLS. 1999; 55(3):494–505. doi: 10.1007/s000180050306.

Wang G, Wyskiel DR, Yang W, Wang Y, Milbern LC, Lalanne T, Jiang X, Shen Y, Sun QQ, Zhu JJ. An optogenetics-and imaging-assisted simultaneous multiple patch-clamp recording system for decoding complex neural circuits. Nature protocols. 2015; 10(3):397. doi: 10.1038/nprot.2015.019.

Westendorf C, Negrete J, Bae AJ, Sandmann R, Bodenschatz E, Beta C. Actin cytoskeleton of chemotactic amoebae operates close to the onset of oscillations. Proceedings of the National Academy of Sciences. 2013; 110(10):3853–3858. doi: 10.1073/pnas.1216629110.

Williams JC, Xu J, Lu Z, Klimas A, Chen X, Ambrosi CM, Cohen IS, Entcheva E. Computational Optogenetics: Empirically-Derived Voltage- and Light-Sensitive Channelrhodopsin-2 Model. PLOS Computational Biology. 2013 09; 9(9):1–19. doi: 10.1371/journal.pcbi.1003220.

Winfree AT. The geometry of biological time, vol. 12. Springer Science & Business Media; 2001. doi: 10.1007/978-1-4757-3484-3.

Xiong L, Garfinkel A. Are physiological oscillations physiological? The Journal of Physiology. 2023; .

Appendix 1

Supplementary Methods

Simplified reaction-diffusion model

The simplified reaction-diffusion model consists of one voltage variable, two gating variables for the depolarising and hyperpolarising currents, and an inhomogeneity parameter $C(x, y)$:

$$\frac{\partial V}{\partial t} = D\Delta V - 6(1 + e^{-\frac{(45+V)}{6.5}})^{-3} j^2 (V - 62.84) \tag{2}$$

$$- (1 + e^{\frac{V+9}{22.4}})^{-1} x_r 0.011536(V + 86.8358) \tag{3}$$

$$- 0.6 I_{K1} - 0.24(10.6408 - 14.6408 e^{\frac{-V}{42.7671}}) C(x, y) \tag{4}$$

$$\frac{\partial j}{\partial t} = \frac{(j_\infty(V) - j)}{\tau_j(V)} \tag{5}$$

$$\frac{\partial x_r}{\partial t} = \frac{(x_{r_\infty}(V) - x_r)}{\tau_j(V)} \tag{6}$$

where D is the diffusion coefficient equal to 0.0003 cm^2/ms. The I_{K1} current formulation was copied from ***Majumder et al.*** (***2016***). The $C(x, y)$ was set to 0.1518115 inside the illuminated square and to 0 outside this. $j_\infty(V), x_{r_\infty}(V), \tau_j(V), \tau_j(V)$ are described as:

$$j_\infty(V) = (1 + e^{\frac{(68+V)}{6.07}})^{-1} \tag{7}$$

$$x_{r_\infty}(V) = (1 + e^{\frac{-(21.5+V)}{7.5}})^{-1} \tag{8}$$

$$\tau_{x_r}(V) = \begin{cases} 2(\frac{0.00061(V+38.9)}{e^{0.145(V+38.9)}-1} + \frac{0.00138(V+14.2)}{1-e^{-0.123(V+14.2)}})^{-1}, V > -57 \\ 4(\frac{0.00061(V+38.9)}{e^{0.145(V+38.9)}-1} + \frac{0.00138(V+14.2)}{1-e^{-0.123(V+14.2)}})^{-1}, V \leq -57 \end{cases} \tag{9}$$

$$\tau_j(V) = \begin{cases} 11.63(1 + e^{-0.1(V+32)}) e^{2.535*10^{-7}V}, V \geq -40 \\ 3.49(\frac{-127140(V+37.78)}{1+e^{0.311(V+79.23)}} e^{0.2444V} - \frac{3.474}{10^5 e^{0.04391*V}} + \frac{0.1212 e^{-0.01052*V}}{1+e^{0.1378(V+40.14)}})^{-1}, V < -40 \end{cases} \tag{10}$$

$$\tag{11}$$

The forward Euler method was used to integrate the equations with a time step $\Delta t = 0.01ms$ and a centered finite-differencing scheme to discretise the Laplacian with a space step of $\Delta x = 0.0625mm$. The total computational domain size was 256 × 256 grid points while the square with the "background" current consisted of 80 × 80 grid points. To create stationary initial conditions, the model was integrated for 2 minutes before a train of stimuli was applied from the upper border of the domain.

Appendix 2

Supplementary Figures

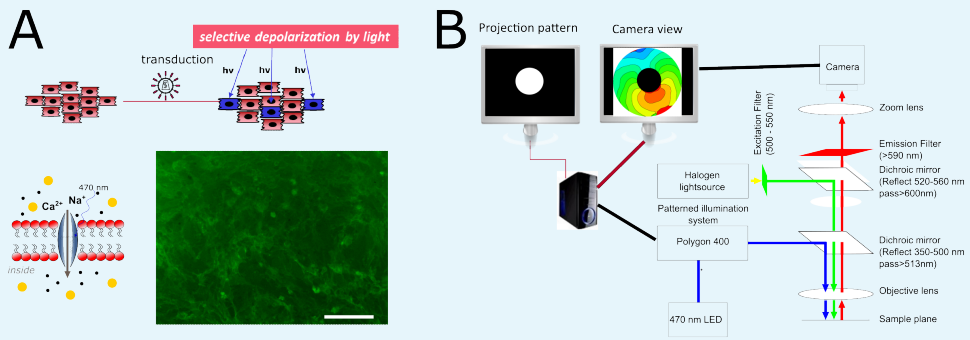

Figure 1. Experimental set-up. (A) Diagrams of the *in vitro* model of NRVMs expressing a light-gated ion channel (top) and of the depolarising light-gated ion channel CheRiff (bottom) together with a representative example of the cell surface fluorescence produced by the enhanced yellow fluorescent protein tag attached to the C terminus of the light-gated ion channel in a CheRiff-expressing NRVM monolayer. **(B)** Optical voltage mapping setup including mapping computer, patterned illuminator (Polygon 400), and optical mapping camera.

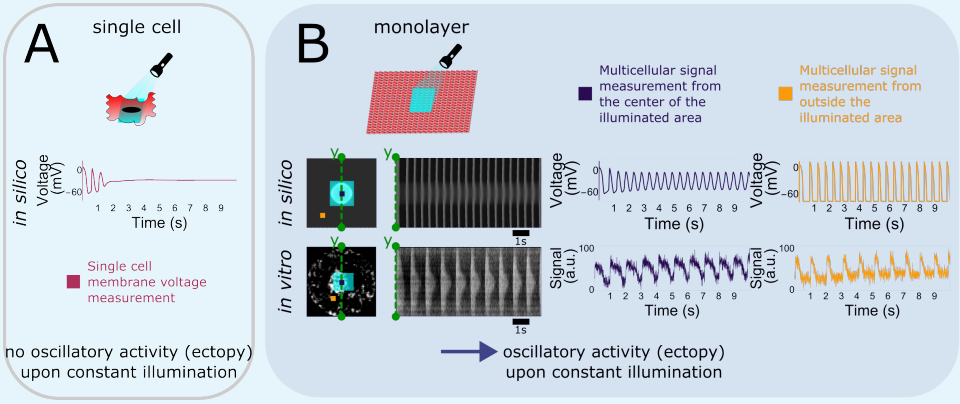

Figure 2. Optogenetic depolarising tools and ectopy. (A) Single cell computational data for application of an optogenetic depolarising tool under constant light illumination, showing a steady depolarised state and lack of sustained oscillations in transmembrane voltage. **(B)** Computational and experimental data showing emergence of ectopic activity in a coupled multicellular system. Sustained ectopic activity emanates periodically from the inside (center) of the illuminated area (light blue box) in both the computational and the experimental model. The sampling positions inside and outside of the illuminated area are indicated by purple and orange squares, respectively. The *in silico* light intensity was the same as in (A).

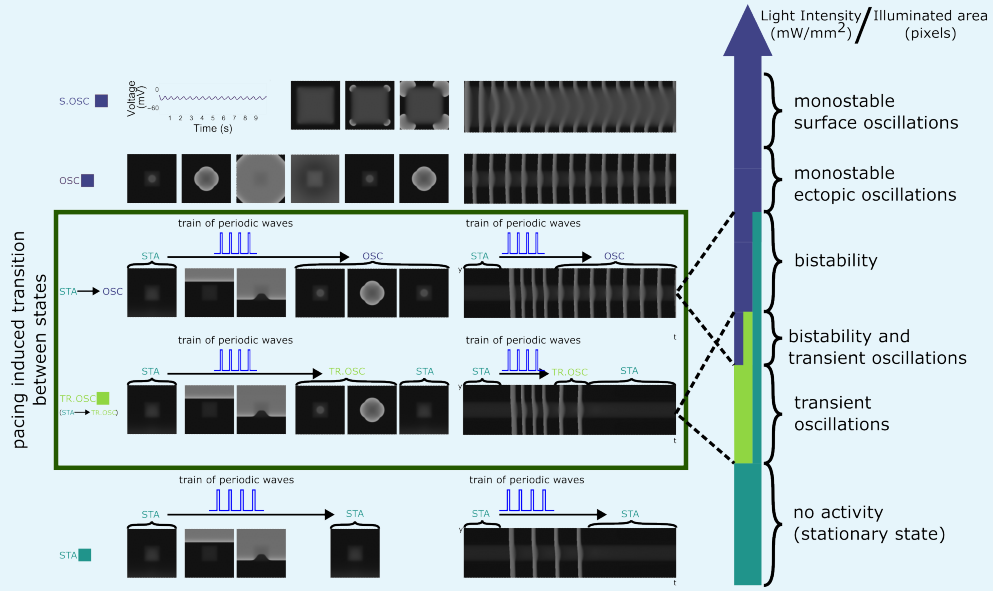

Figure 3. A range of collective phenomena are observed in a multicellular *in silico* NRVM model. Exposure of a squared region in the center of the NRVM monolayer to light of different intensities generates of a photocurrent of different strength by the light-gated depolarising ion channel. Application of a periodic wave train to these NRVM monolayers results in 5 different outcomes, which are each visualised by representative snapshots and a linear time-extract. Going from a high (top) to low (bottom) light intensity these outcomes are: (1) monostable surface oscillations, S.OSC, (2) monostable ectopic oscillations, OSC, (3) bi-stability, (4) transient oscillations, TR.OSC, and (5) stationary state with no activity, STA.(1). The bi-stability region (STA->OSC) and the transient oscillations (STA->TR.OSC) (green box) are described in the main manuscript and supplemental material of this manuscript, respectively.

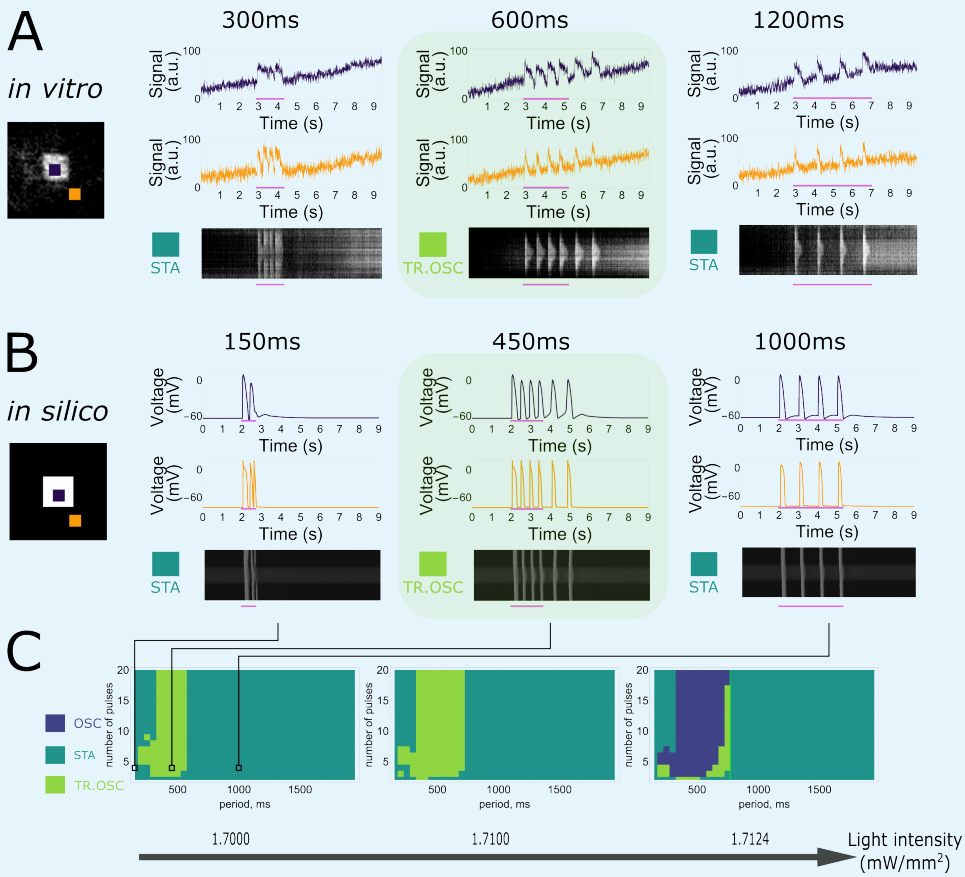

Figure 4. Frequency dependency of transient pacemaker activity induction. (A) *In vitro* monolayers of optogenetically modified NRVMs show that the transition from the stationary state (STA) towards the transient oscillatory state (TR.OSC) is dependent on the frequency of excitatory waves passing through an illuminated area under a constant number of 4 pulses. Four pulses at a high frequency (300-ms period) or low frequency (1200-ms period) do not induce the transition in contrast to 4 pulses with an intermediate period of 600 ms. **(B)** Qualitative correspondence of this behaviour is shown in a computational NRVM model for low (1000-ms period), intermediate (450-ms period), and high (150-ms period) stimulation frequencies. **(C)** Slices of the full parameter plot for a constant size of the illuminated central region of the optogenetically modified NRVM monolayer (80×80 pixels) with indications of the selected frequency visualisations.

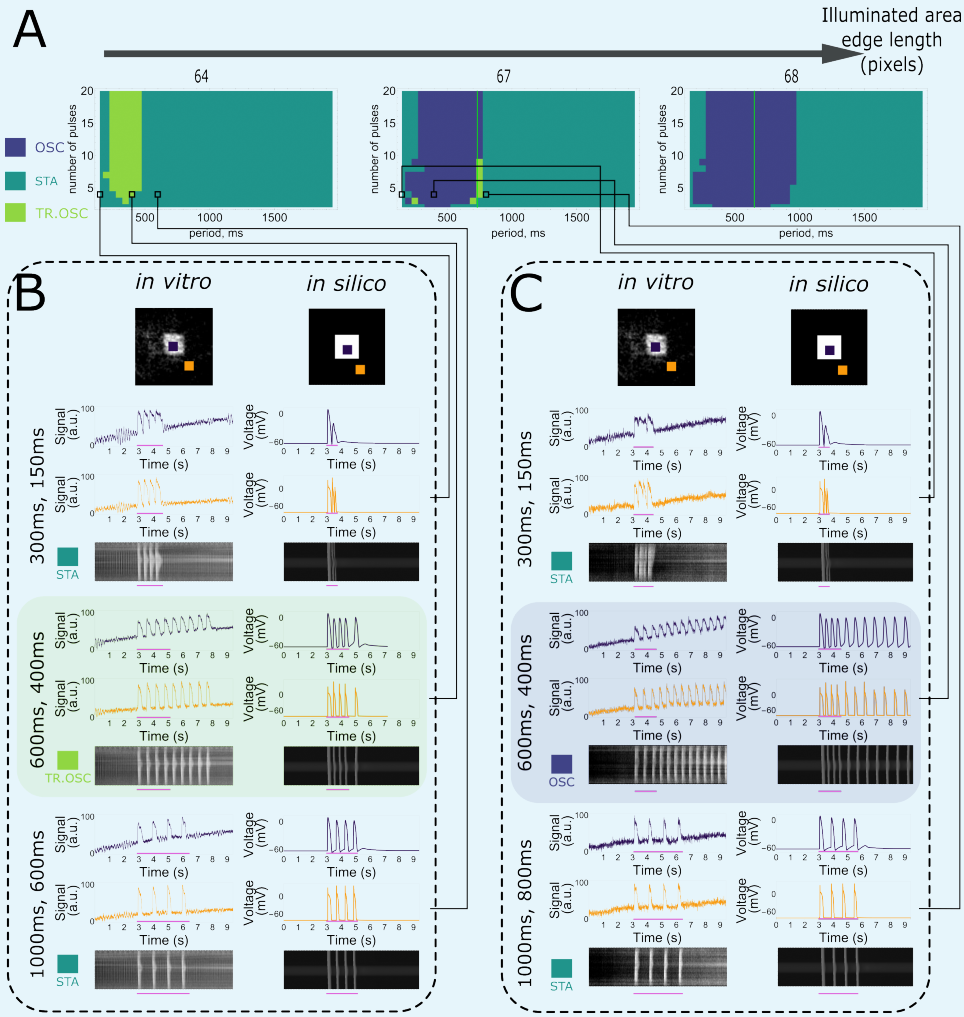

Figure 5. Influence of the size of the illuminated central square on transient pacemaker activity induction. (A) Slices of the full parameter plot for constant illumination (1.72 mW/mm^2) with indications of selected frequency visualisations. **(B)** Transient oscillations can be induced with a small-sized illumination region (64×64 pixels) for intermediate frequencies. **(C)** The oscillatory state can be induced with a large-sized illumination region (67×67 pixels) for intermediate frequencies.

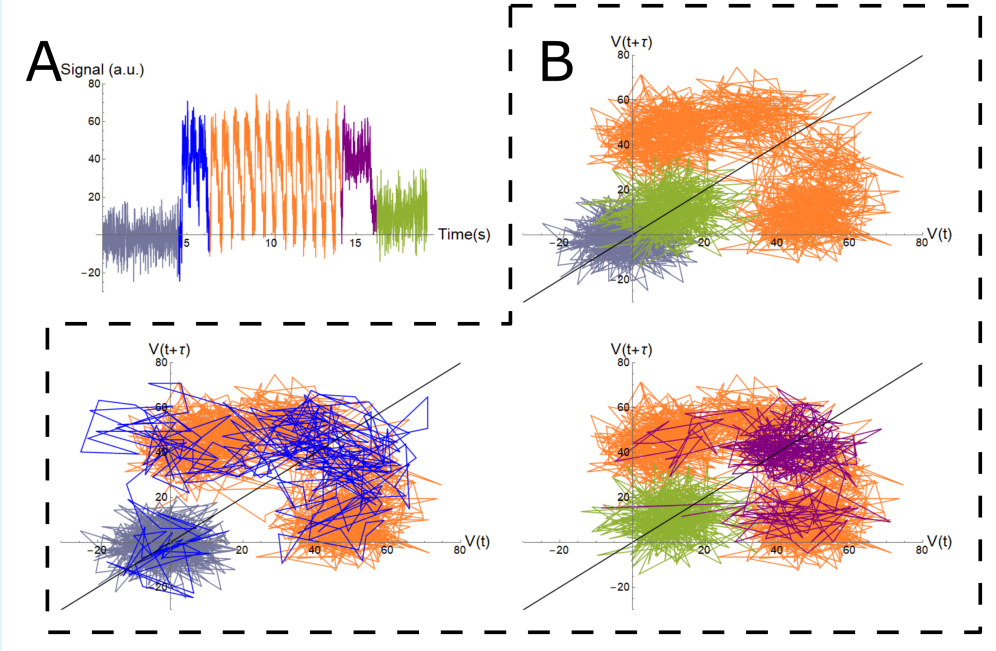

Figure 6. Trajectory reconstruction using Takens time delay embedding. (A) The optical voltage signal shows induced initiation and termination of pacemaker activity. The initial stationary state is shown in grey, the initiating stimulating pulses in blue, periodic oscillations in orange, the terminating high frequency stimulation in purple, and the stationary state after termination of oscillatory pacemaker activity in light green. **(B)** Trajectories in phase space in $(V(t), V(t+\tau))$ coordinates showing multiple attractors (grey/green [STA]) and orange [OSC]) and the transition between them (blue/purple).

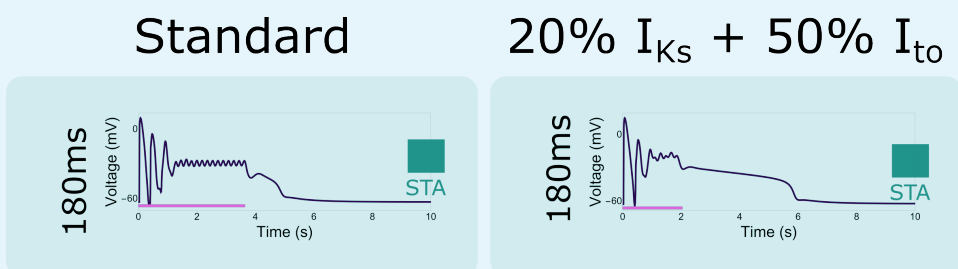

Figure 7. The effect of ionic changes on the termination of pacemaker activity The mechanism that moves the oscillating illuminated tissue back to the stationary state after high frequency pacing is dependent on the ionic properties of the tissue, i.e. higher repolarisation reserves (20% I_{Ks} + 50% I_{to}) are associated with longer transition times.

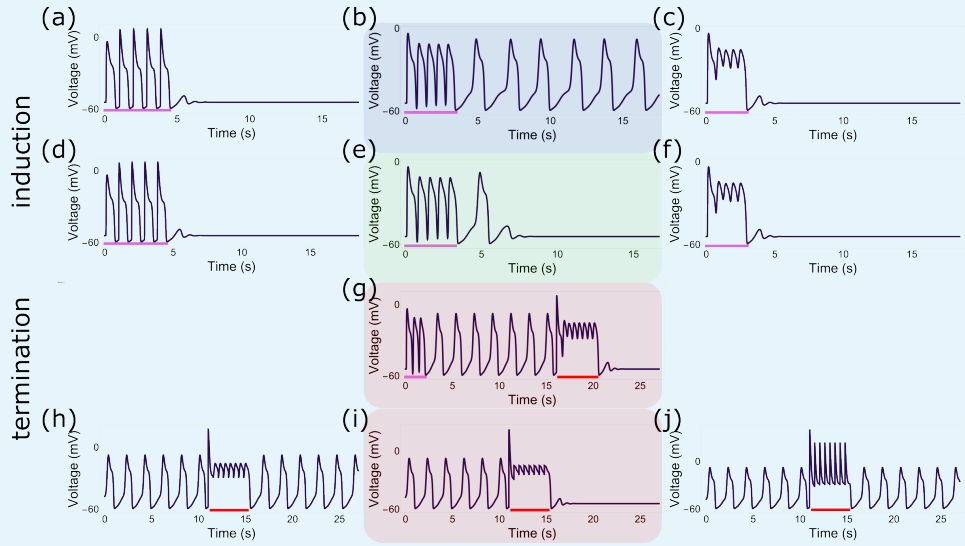

Figure 8. Qualitative similarities between the simplified and complex reaction-diffusion model. (a-c) Five pulses of low and high frequency fail to induce pacemaker activity in the simplified *in silico* NRVM model, while intermediate frequencies do. (d-f) Under lower illumination intensity, five pulses of low and high frequency fail to induce pacemaker activity, while intermediate frequencies induce transient oscillations. (g) Termination of pacemaker activity by high frequency travelling waves of excitation. (h-j) Failure to terminate pacemaker activity by spatially uniform voltage perturbations of high frequency and low (-30 mV) or high (50 mV) magnitude, while termination is successful at an intermediate magnitude of -20 mV).

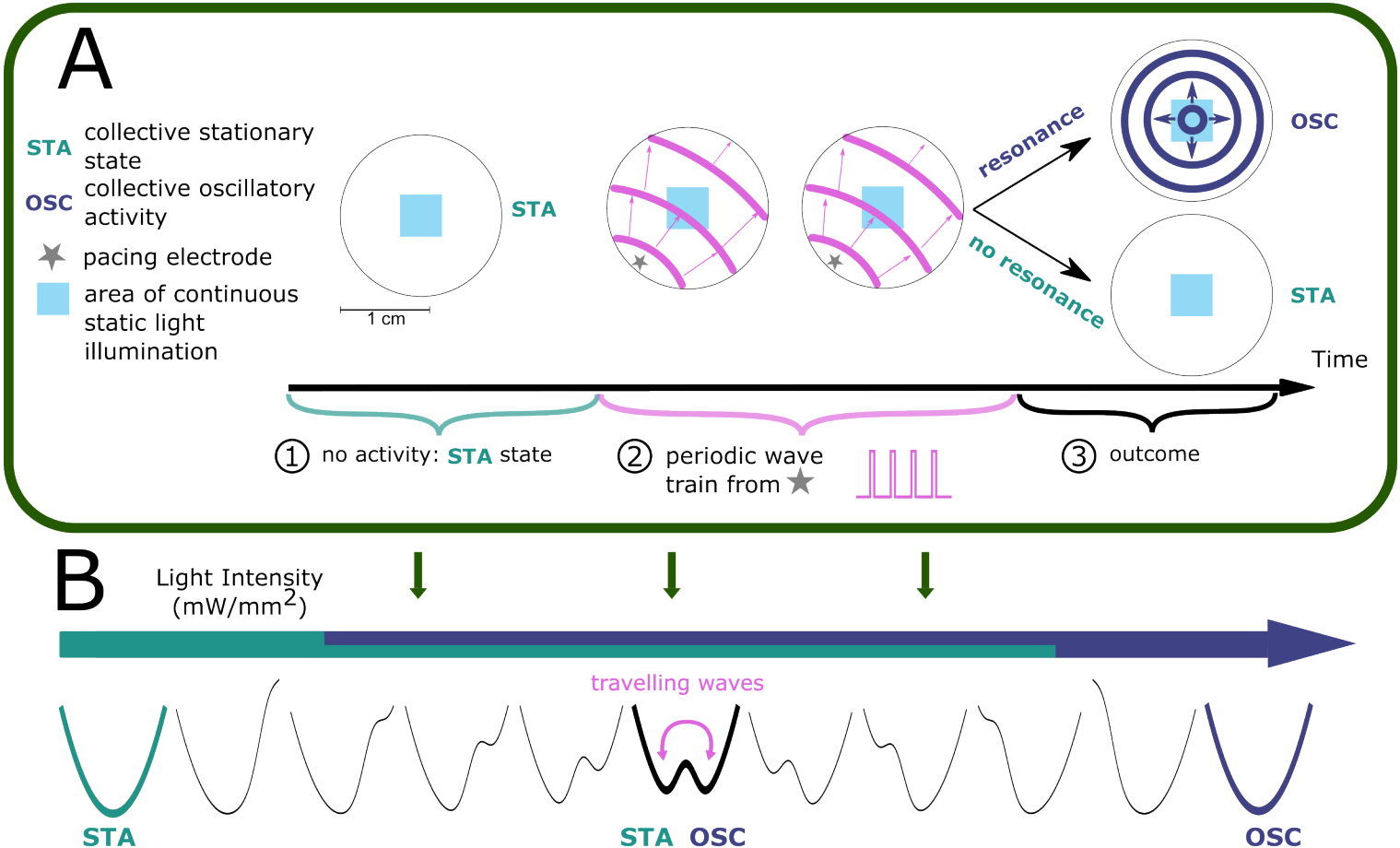
A
STA collective stationary state
OSC collective oscillatory activity
pacing electrode
area of continuous static light illumination
STA
1 cm
resonance
no resonance
OSC
STA
Time
① no activity: STA state
② periodic wave train from
③ outcome
B
Light Intensity (mW/mm2)
travelling waves
STA
STA OSC
OSC

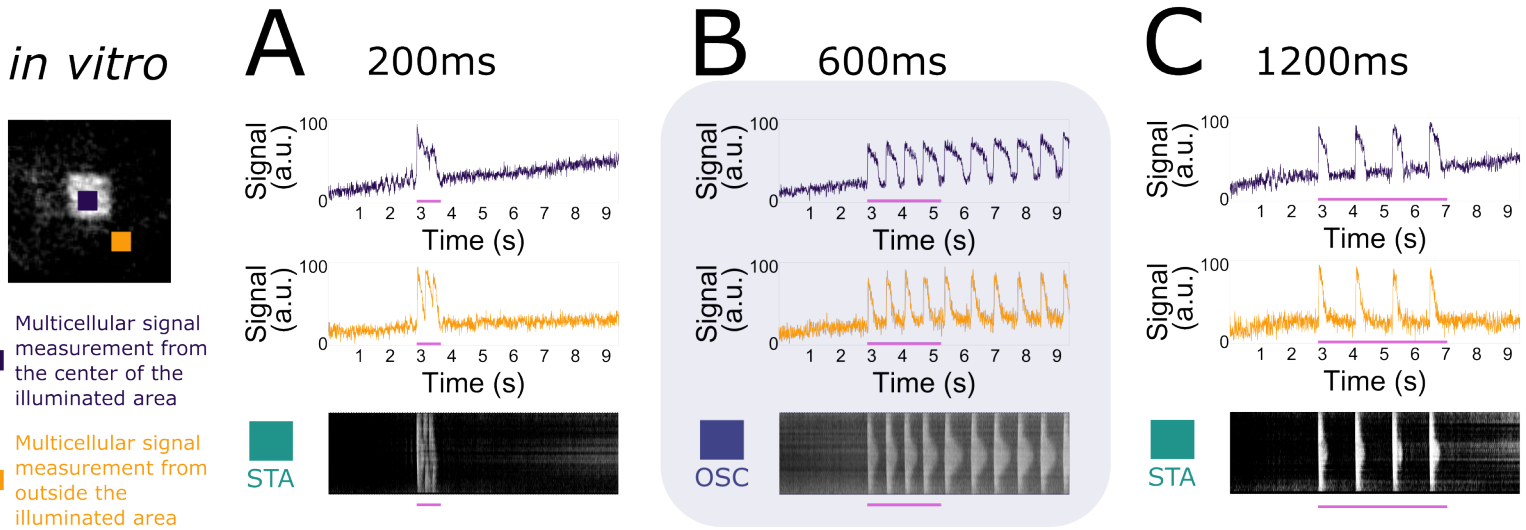
in vitro
A
200ms
B
600ms
C
1200ms
Signal (a.u.)
100
0
1 2 3 4 5 6 7 8 9
Time (s)
Multicellular signal measurement from the center of the illuminated area
Multicellular signal measurement from outside the illuminated area
STA
OSC
STA

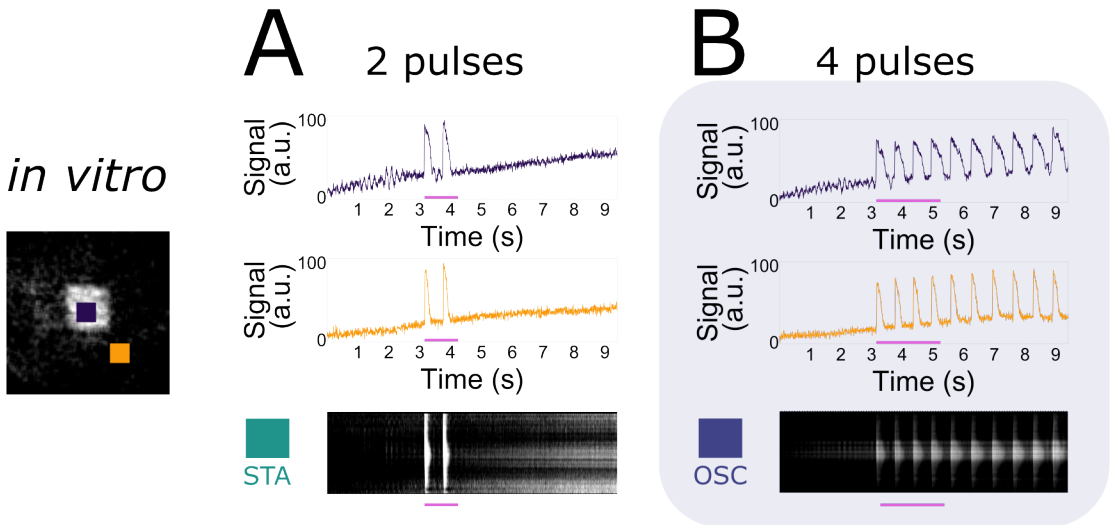
A
2 pulses
B
4 pulses
in vitro
Signal (a.u.)
100
0
1 2 3 4 5 6 7 8 9
Time (s)
STA
OSC

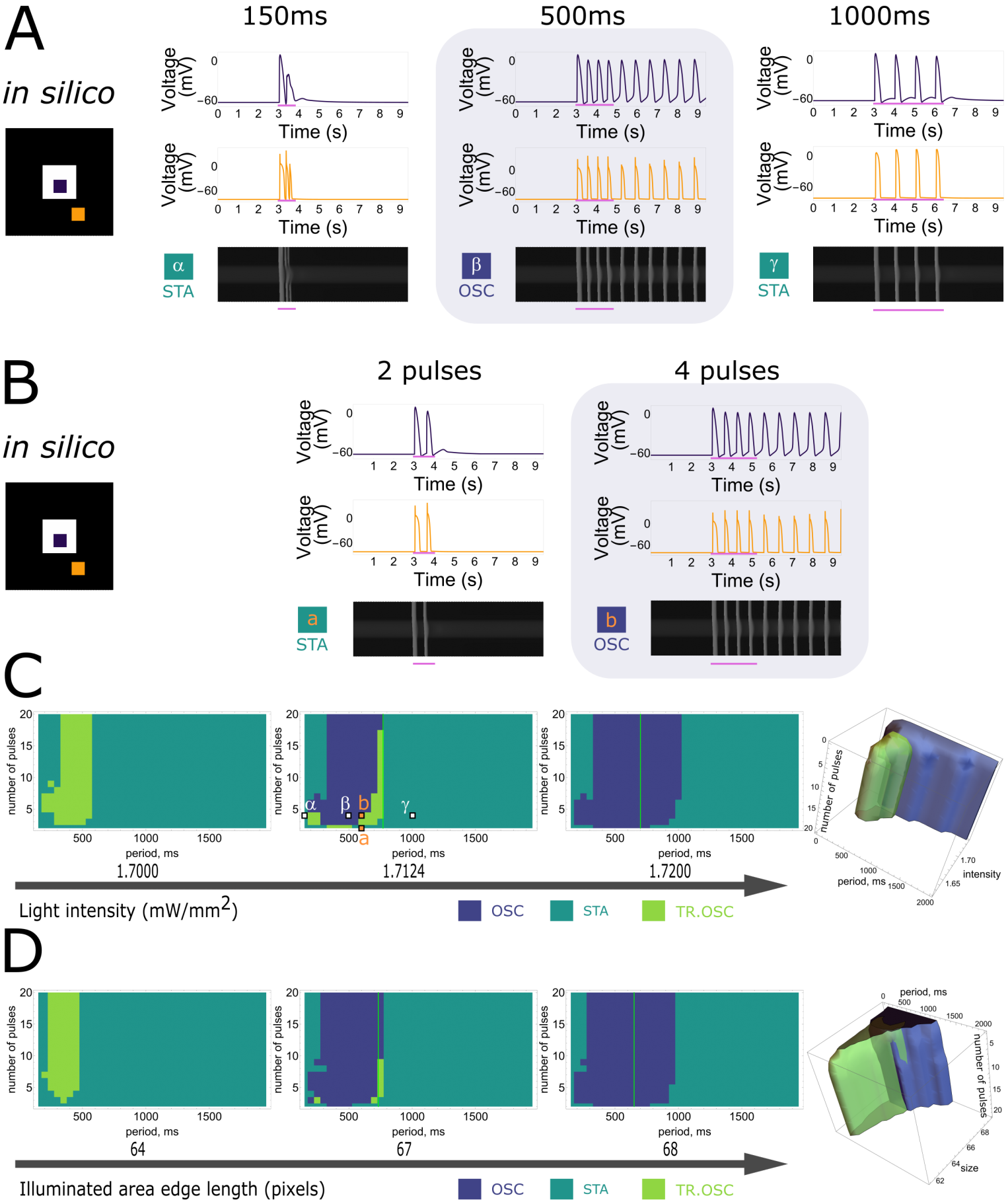
A
in silico
150ms
500ms
1000ms
Voltage (mV)
Time (s)
α
STA
β
OSC
γ
STA
B
in silico
2 pulses
4 pulses
a
STA
b
OSC
C
number of pulses
period, ms
1.7000
1.7124
1.7200
Light intensity (mW/mm2)
OSC
STA
TR.OSC
D
64
67
68
Illuminated area edge length (pixels)
OSC
STA
TR.OSC

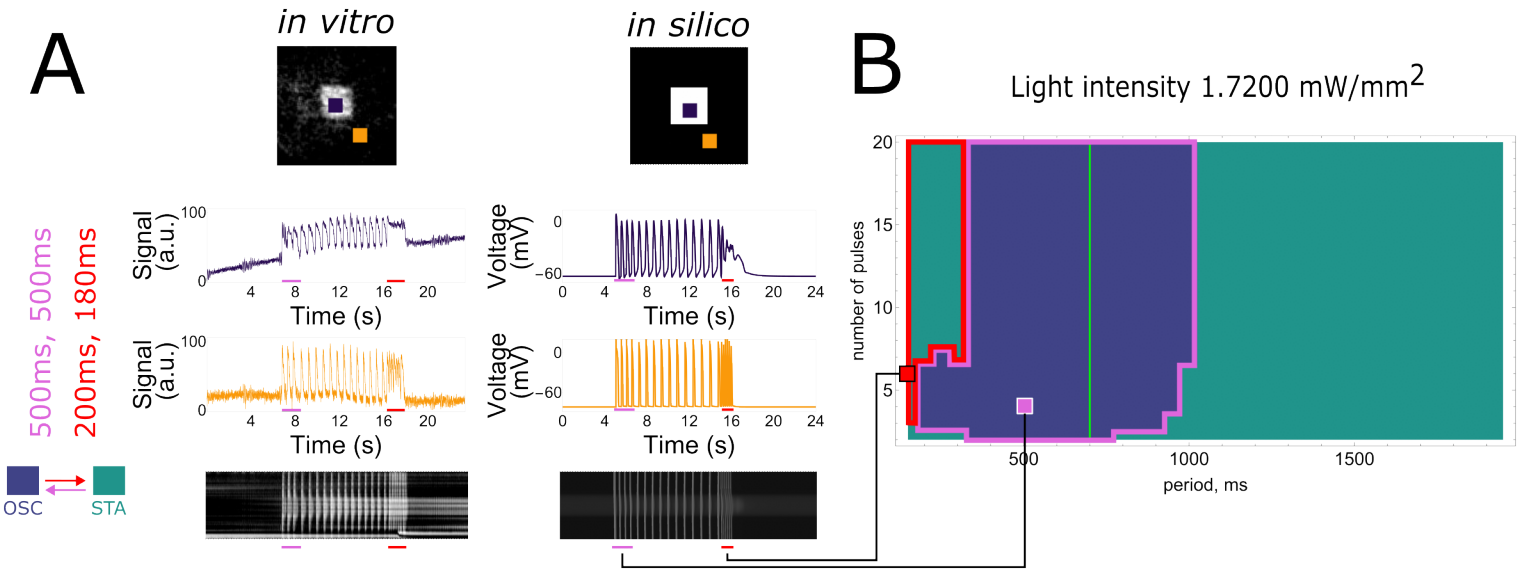
A
in vitro
in silico
B
Light intensity 1.7200 mW/mm2
500ms, 500ms
200ms, 180ms
OSC
STA
Signal (a.u.)
Voltage (mV)
Time (s)
number of pulses
period, ms

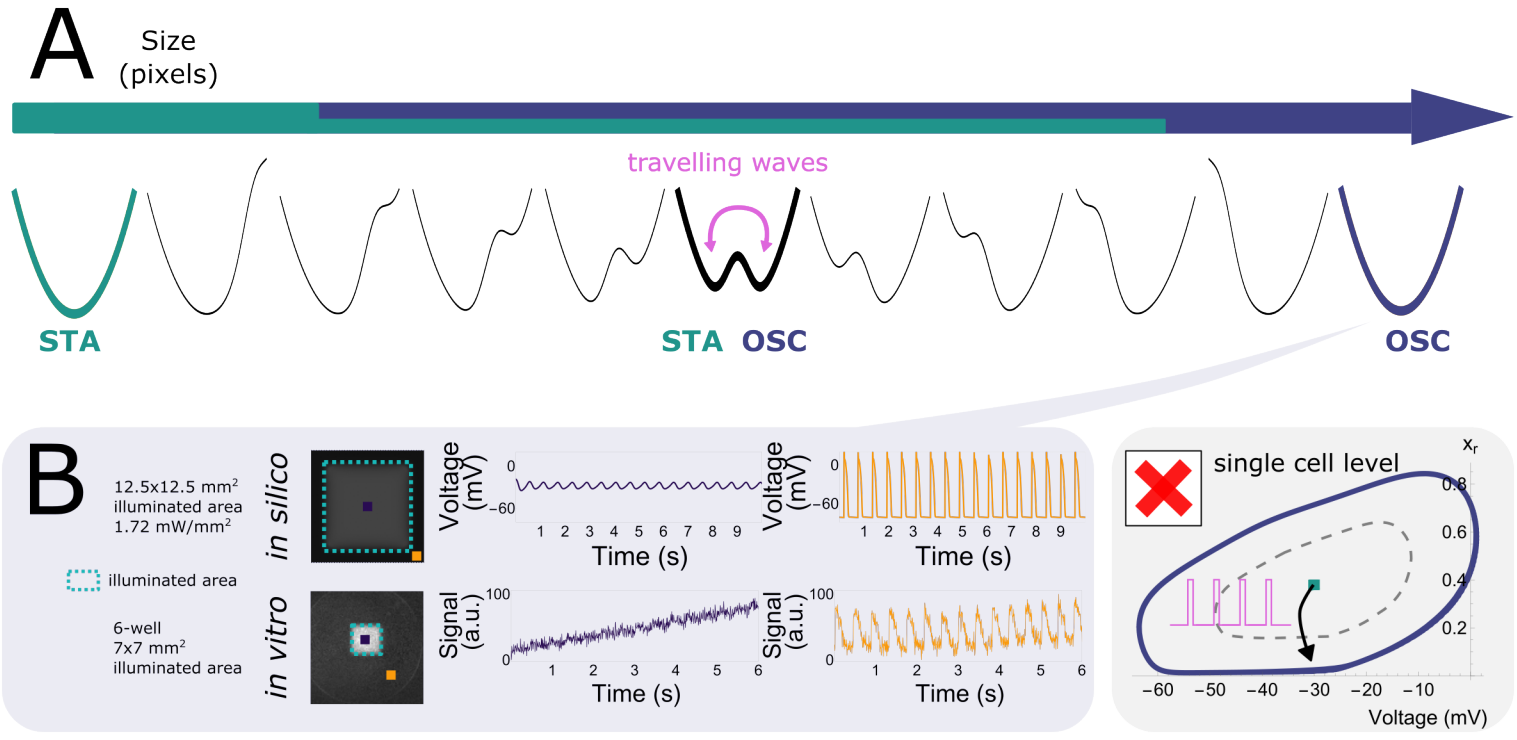
A
Size
(pixels)
travelling waves
STA
STA OSC
OSC
B
12.5x12.5 mm²
illuminated area
1.72 mW/mm²
illuminated area
6-well
7x7 mm²
illuminated area
in silico
in vitro
Voltage (mV)
0
−60
1 2 3 4 5 6 7 8 9
Time (s)
Signal (a.u.)
100
0
1 2 3 4 5 6
Time (s)
single cell level
x_r
0.8
0.6
0.4
0.2
−60 −50 −40 −30 −20 −10
Voltage (mV)

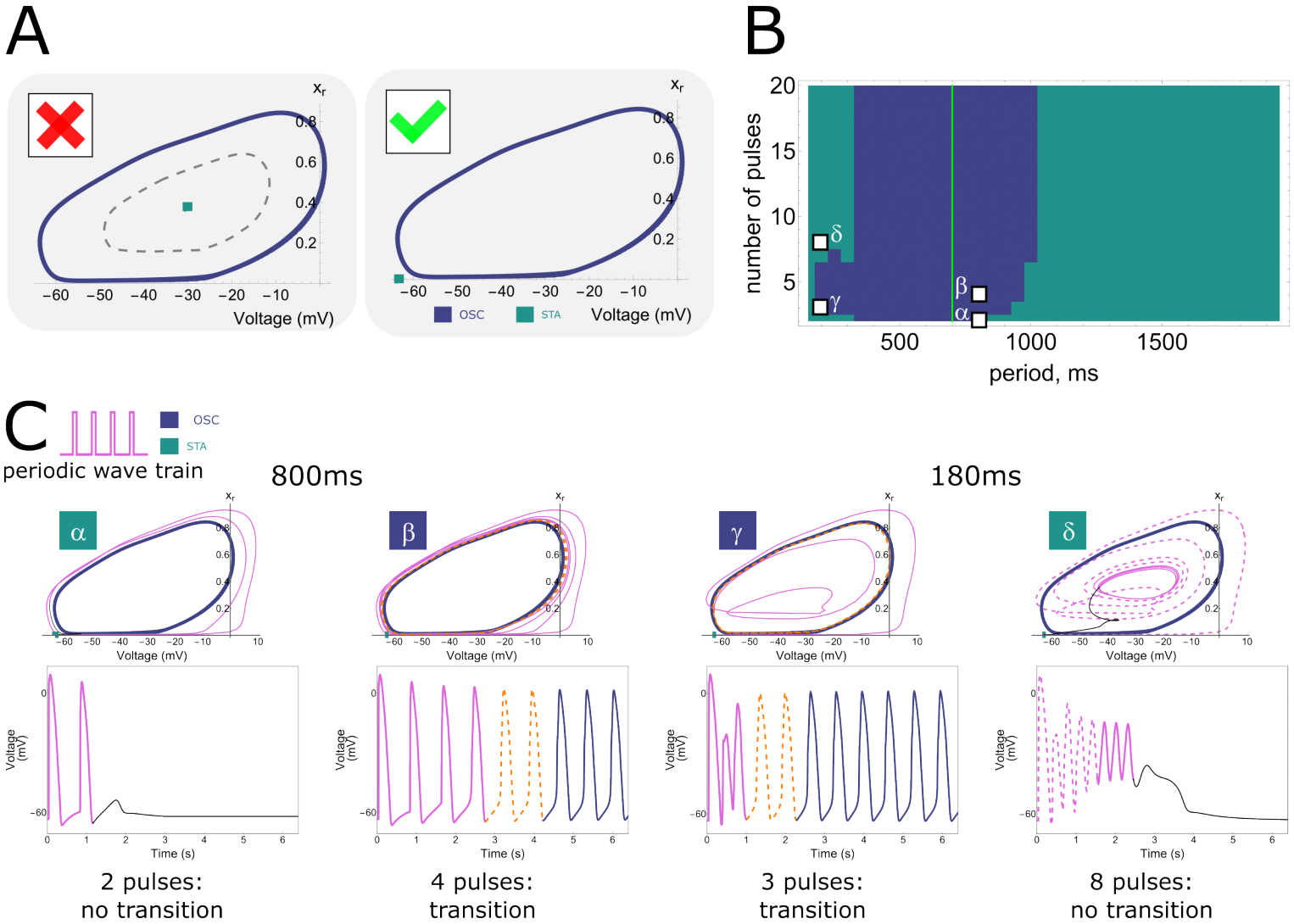
A
B
C
x_r
Voltage (mV)
OSC
STA
number of pulses
period, ms
periodic wave train
800ms
180ms
α
β
γ
δ
Time (s)
2 pulses:
no transition
4 pulses:
transition
3 pulses:
transition
8 pulses:
no transition

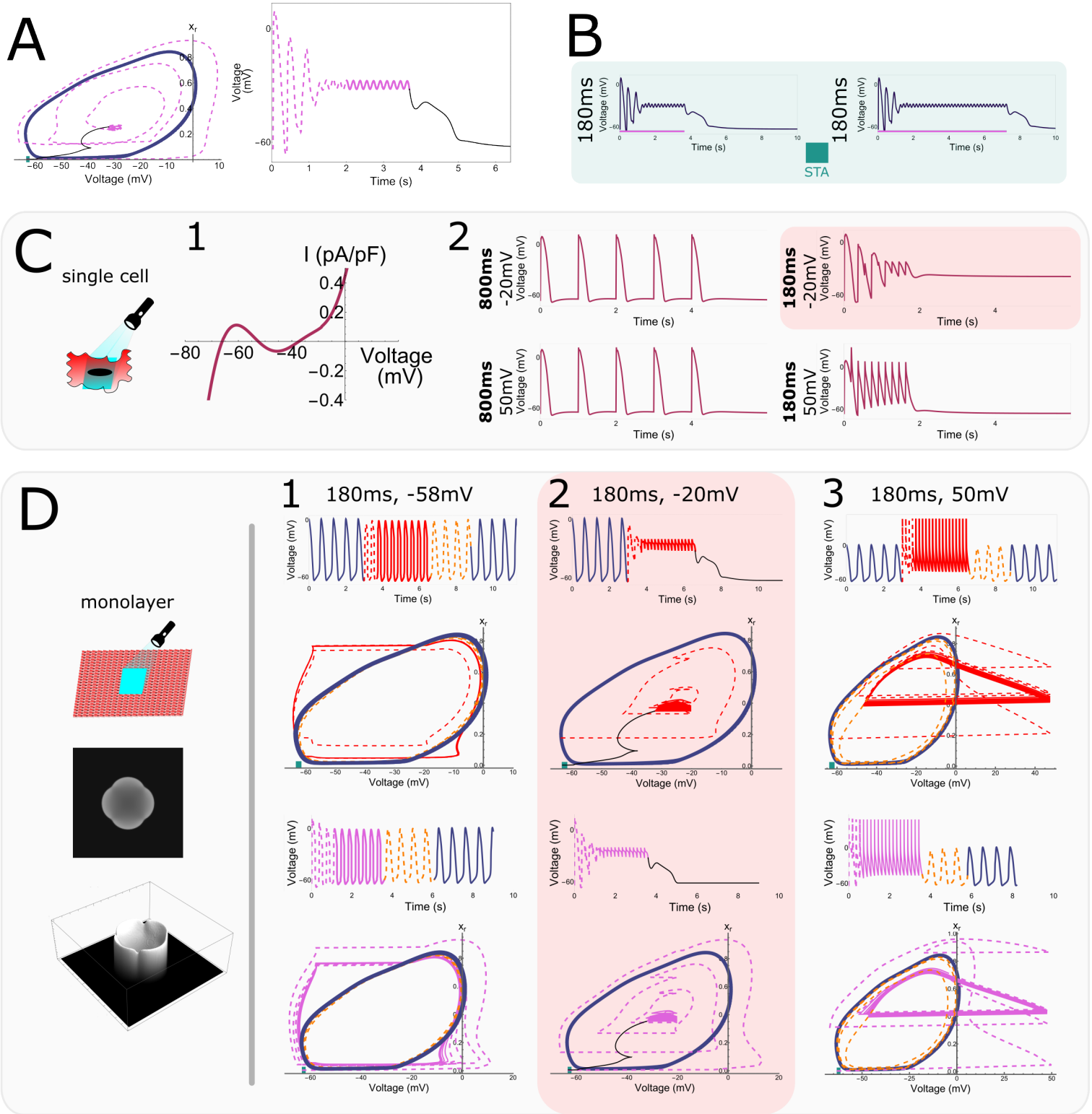
A
Voltage (mV)
Time (s)
B
180ms
STA
C
single cell
1
I (pA/pF)
Voltage (mV)
2
800ms -20mV
180ms -20mV
800ms 50mV
180ms 50mV
Time (s)
D
monolayer
1 180ms, -58mV
2 180ms, -20mV
3 180ms, 50mV
Voltage (mV)
Time (s)

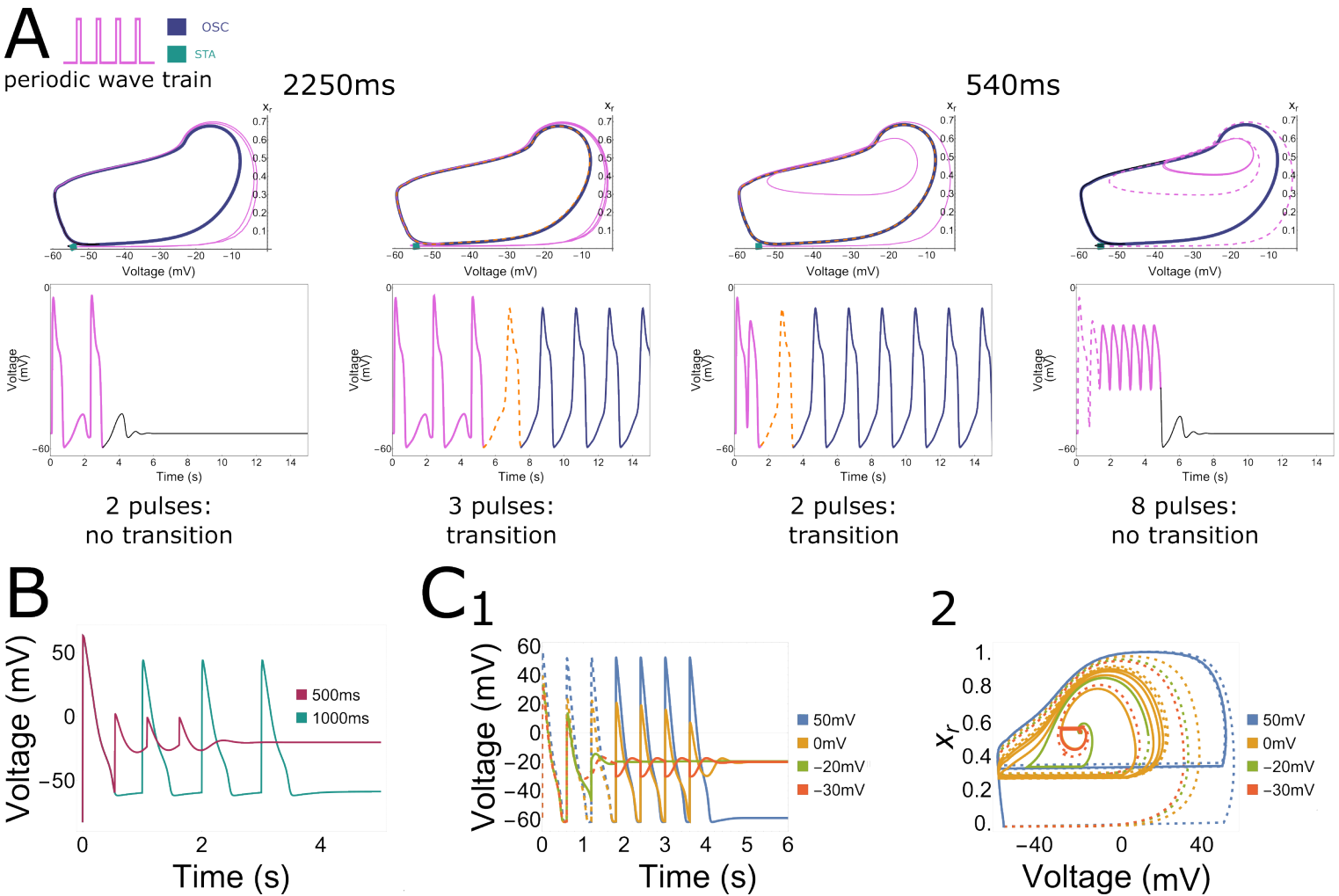
A
OSC
STA
periodic wave train
2250ms
540ms
Voltage (mV)
Time (s)
2 pulses:
no transition
3 pulses:
transition
2 pulses:
transition
8 pulses:
no transition
B
500ms
1000ms
Voltage (mV)
Time (s)
C1
50mV
0mV
−20mV
−30mV
Voltage (mV)
Time (s)
2
50mV
0mV
−20mV
−30mV
Voltage (mV)